Study on $(Bi_{1-y}B_yS)_n$ $(Ti_{1-x}A_xS_2)_2$ Misfit Layer Sulfide as a Novel Thermoelectric Material

Yulia Eka Putri

480911118

Department of Applied Chemistry,
Chemical Engineering and Biotechnology
Graduate School of Engineering
Nagoya University
2013

平成 25 年度博士論文

Study on $(Bi_{1-y}B_yS)_n$ $(Ti_{1-x}A_xS_2)_2$ Misfit Layer Sulfide as a Novel Thermoelectric Material

名古屋大学大学院
工学研究科
化学・生物工学専攻
応用化学分野
D3
ユリアエカプトリ
（Yulia Eka Putri）

ABSTRACT

We report on the study of $(Bi_{1-y}B_yS)_n$ $(Ti_{1-x}A_xS_2)_2$ misfit layer sulfide as a novel thermoelectric material. This research is motivated by the problem of availability of the energy in the future as energy resources derived from fossil fuels will be reduced along with the increasing demand for energy. Fossil fuel that is used as the primary energy in daily lives will produce secondary energy, one third of which can be used to meet demand but the rest is wasted, especially in the form of heat dissipated into air. It would be better if the waste heat can be converted directly into electricity, so that it can be used immediately and diminished human concern on the insufficient of energy.

Thermoelectric power generator is considered as a green solution for energy recovery because this module can harvest waste heat and directly convert it into electricity by utilizing the Seebeck effect. The thermoelectric material performance is evaluated by the dimensionless figure of merit, $ZT = S^2\sigma T/\kappa$, where S, σ and κ are Seebeck coefficient, electrical conductivity and thermal conductivity, respectively, at a given absolute temperature, T. The thermoelectric energy conversion efficiency is a function of ZT value and high ZT value results high energy conversion efficiency. Therefore, to achieve high ZT value, Seebeck coefficient (S) and electrical conductivity (σ) should be high simultaneously while the thermal conductivity (κ) should be low.

In this research, we are focusing on n-type thermoelectric material which is naturally abundant, non toxic, oxidation resistant and cost effective. TiS_2 has shown its potential as a promising thermoelectric material through its high power factor ($S^2\sigma$) at room temperature. However, its TE performance is limited by its high thermal conductivity (κ), so that the ZT value is not optimal. The intercalation of metal sulfide (PbS, SnS, BiS) as a phonon barrier layer into the van der Waals gaps forming $(MS)_{1.2}(TiS_2)_2$ misfit layer sulfide has become an effective way in reducing the thermal conductivity. However, reducing the thermal conductivity in this manner does not increase the ZT value very much; electron transfer from BiS layers to TiS_2 layers increases the carrier concentration, largely increasing the electrical conductivity and

electronic thermal conductivity. As a result, the Seebeck coefficient decreases and the power factor could not be optimized. Among these metal sulfides, we selected $(BiS)_{1.2}(TiS_2)_2$ misfit layer sulfide because this compound has the lowest lattice thermal conductivity and has the highest potential to achieve a high *ZT* value if the carrier concentration could be suitably controlled. We seek for the possibility to enhance the thermoelectric performance of this material through reduction of carrier concentration while maintaining the low lattice thermal conductivity.

We propose a strategy, so-called modulation/selective doping, by substituting an acceptor dopant into the different lattice sites of $(BiS)_{1.2}(TiS_2)_2$. First, we selected the acceptor dopants from alkaline earth (AE) element (Mg, Ca, Sr). Magnesium ($Mg^{2+)}$ substitutes the titanium (Ti^{4+}) sites forming $(BiS)_{1.2}(Ti_{0.95}Mg_{0.05}S_2)_2$ while strontium (Sr^{2+}) and calcium (Ca^{2+}) for bismuth (Bi^{3+}) sites forming $(Bi_{0.9}Sr_{0.1}S)_{1.2}(TiS_2)_2$ and $(Bi_{0.9}Sr_{0.1}S)_{1.2}(TiS_2)_2$.

The samples were prepared by a solid-state reaction method and the thermoelectric measurement was conducted in the direction perpendicular with the pressure applied during densification (in-plane). The structural analysis by XRD shows that the samples have a strong preference for an orientation with the *c* axis parallel to the pressure and no substantial changes or secondary phases were observed after doping. The alkaline earth (AE) elements substitution did reduce the carrier concentration and electrical conductivity. However, the Seebeck coefficient decreased slightly due to the decrease in effective mass of carrier electrons. As a result the power factor is not optimal. We have confirmed that the formation of ordered structure in the magnesium doped sample and the assumption of the alteration of incommensurate to commensurate structure in the calcium and strontium doped samples led to an increase in lattice thermal conductivity. The formation of structural ordering increases the phonon mean free path, allowing the phonons to easily pass through the lattice, as a result the lattice thermal conductivity is enhanced.

We continued to search for other promising dopants from the transition metal (TM) elements (V, Cr, Mn, Fe, Co, Ni, Cu and Zn). These dopants substitute for titanium (Ti^{4+}) sites forming $(BiS)_{1.2}(Ti_{0.95}TM_{0.05}S_2)_{2.}$ The XPS measurement shows that all the transition metal ions have been successfully substituted for Ti^{4+} in the TiS_2 layers. All

the transition metal substitution successfully reduced the carrier concentration, but we lkm;discovered that only vanadium and chromium-doped sample led to a significant increase in the Seebeck coefficient while the other TM doped samples decrease it. We demonstrated that besides the reduction of carrier concentration, the enhancement in the Seebeck coefficient of V and Cr-doped sample is due to the increase in the effective mass of carriers. Though TiS_2 is a narrow-band gap semiconductor, $(BiS)_{1.2}(TiS_2)_2$ possibly becomes a semi-metal, due to the overlap of the broad band of the BiS sub-layer and the band of the TiS_2 sub-layer. Therefore, a reduction of carrier concentration does not necessarily to increase the Seebeck coefficient, as has been shown in our previous study of AE-doped $(BiS)_{1.2}(TiS_2)_{2.}$ However, in the case of V and Cr doping, the low energy level of the doped element is possibly close to the Fermi level and therefore forms a resonance state that can enhance the effective mass and improve the Seebeck coefficient.

The power factor of all TM doped samples could not be improved as the electrical properties could not be optimized. Electronic thermal conductivity was significantly reduced due to the decrease in the electrical conductivity. The increase in the lattice thermal conductivity is caused by the new structural ordering. This new ordering occurs as a result of elimination of planar stacking faults present in the undoped sample.

We realized that further investigation is needed to clarify the mechanism of the increase of Seebeck coefficient in the chromium doped sample. The DFT calculation for the $(BiS)_{1.2}(Ti_{0.9}Cr_{0.1}S_2)_2$ sample confirms that the formation of additional resonant states near Fermi level as a result of chromium doping, which can account for the increase in effective mass. Moreover, the DOS near the Fermi level is mainly contributed by the *3d* orbital of Ti atoms near the Cr dopant. The electronic thermal conductivity is significantly reduced due to the decrease in the electrical conductivity. Consequently, the overall *ZT* value was measurably improved up to 0.3 at 750K.

We conclude that, a suitable dopant which can simultaneously induce additional states around the Fermi level and limit the formation of order structure will significantly enhance the thermoelectric properties $(BiS)_{1.2}(TiS_2)_2$ misfit layer sulfide.

ACKNOWLEDGEMENTS

First and foremost, I am grateful to Almighty Allah SWT for His guidance and blessings throughout my life so that I can realize all dreams and lofty ideals in completing this dissertation. Prophet Muhammad SAW, may he always placed by God on his side as the people who obtained the highest degree in the afterlife.

My deepest respect and sincerest gratitude to my supervisor, Prof.Kunihito Koumoto who has supported me throughout my study with his supervision and knowledge. His invaluable guidance, insightful thinking, constructive criticisms, as well as his enthusiasm in research had inspiring during my study. I also would like to express my gratitude to Dr. Yifeng Wang and Dr. Chunlei Wan for his kind assistance and guidance during my research.

My special thanks to Koumoto laboratory member at Nagoya University for their friendship and making my study life a memorable one. Especially for Namy, thank you for being my lovely friend.

I would also like to convey thanks to Andalas University and Indonesian Government especially Ministry of Education and Culture of Indonesia for giving the opportunity and providing the financial support.

My dearest parents, Ayah and Ibu, thank you for your prayer and persistent love. My beloved brothers and sister and my big family, thank you for your good wishes and support throughout my studies.

My deepest appreciation goes to my beloved husband, Dedi Satria for his sincere love, constant care, encouraging supports and always standing beside me in any circumstances. Hopefully, this achievement makes us always eternally grateful. To my beloved son Avicenn Deska and my beloved daughter Aisha Deska, thank you for your patience and understanding you've given to Bunda. I love you kids!.

Lastly, I offer my regards and gratitude to all of those who supported me in any aspects during my research and the completion of the thesis.

CONTENTS

LIST OF SYMBOLS

E	Electric field
S	Seebeck coefficient
∇T	Temperature gradient
$\prod$	Peltier coefficient
μ_{JT}	Thomson coefficient
μ	Carrier mobility
ZT	Dimensionless figure of merit
σ	Electrical conductivity
ρ	Resistivity
κ	Thermal conductivity
α	Thermal diffusivity
C_P	Specific heat capacity
κ_e	Electrical thermal conductivity
κ_l	Lattice thermal conductivity
n	Carrier concentration
m^*	Effective mass of carriers
η	Thermoelectric generator efficiency
$S^2\sigma$	Power factor
λ	Wavelength
R	Electrical resistance
A	Cross section area of specimen
U	Voltage difference across the probes
I	Current

J	Current density
E_F	Fermi level
k_B	Boltzman constant
h	Plank constant
e	Electric charge
L_o	Lorentz number
V	Sound velocity
V_L	Longitudinal sound velocity
V_T	Transverse sound velocity

Chapter I

Introduction

Energy issues are becoming increasingly complex as the increase of need in energy supply for the human life. The dependence of fossil fuels such as petroleum, natural gas and coal as a primary energy resource has posed a serious threat to the lives of living beings on earth. The threat is not only because of the insufficient of this conventional energy but also its consumption produces a large amount of greenhouse gases, e.g. CO_2, which should be responsible for the continuously rising of the global warming for decades. Therefore, the intensive development and direct implementation of renewable fuels, e.g. wind power, solar cell, biomass, geothermal energy and etc has attempted to solve energy problem. Furthermore, various novel idea and techniques have also been developed to recover and save the energy [1. 2].

The effort in saving energy by converting the waste heat into electricity using thermoelectric (TE) power generation is tremendously attractive. Large amount of heat is released into the environment will be harvested and used directly. TE power generation is constructed and compiled into a module by compactly arrangement of n-type and p-type thermoelectric materials which are connected in series as illustrated in Fig.1-1. This module is very promising for power generation, especially as a heat recovery in vehicle, household and industry.

In addition to power generation, thermoelectric can also be used as refrigeration when the electric current is applied. It gives a significant value for a micro scale electronic device manufacture, using as a portable coolers for cooling electronic components and small instruments [3].

The thermoelectric has several advantages over the others technique:

1. No moving part or rotating part: maintenance-free and long service life.
2. Environmentally friendly: clean (no pollutant), silent operation, simple construction and best suited for emergency power supply at disaster area.

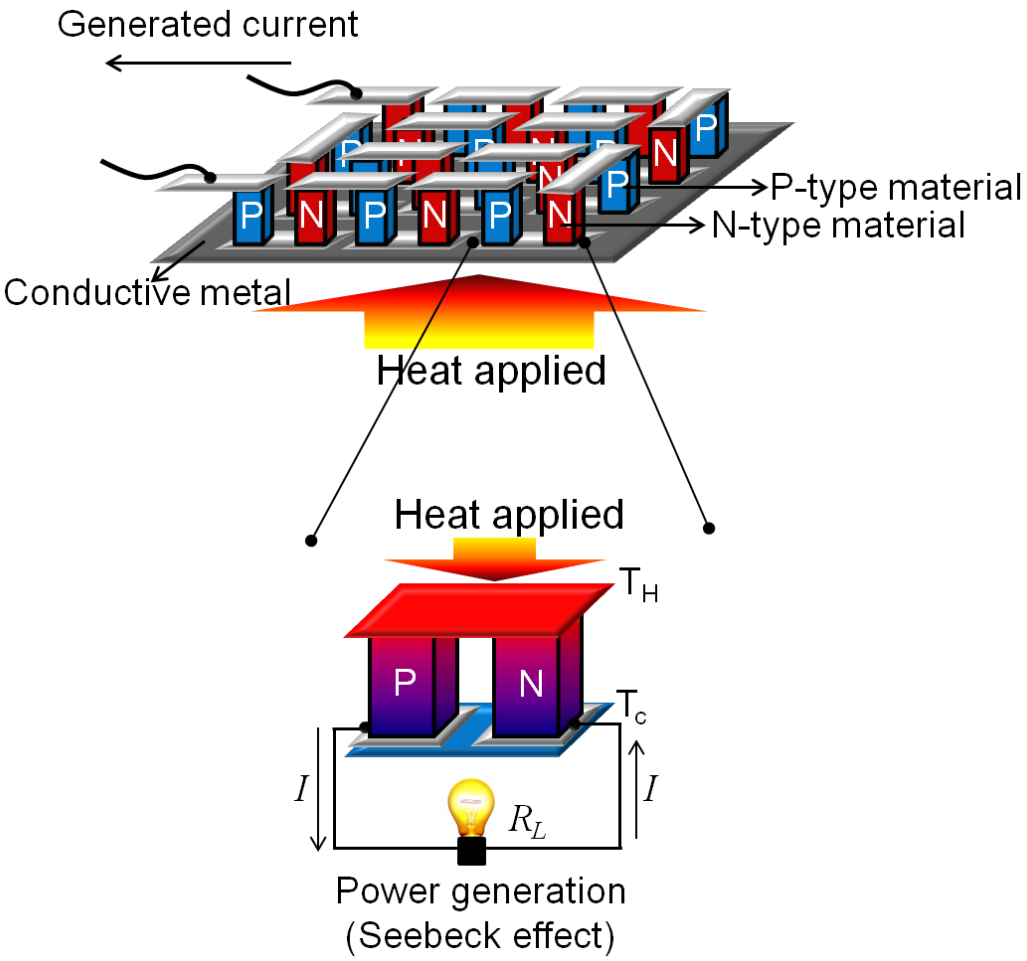

Fig. 1-1. Schematic images of thermoelectric module connected in series (n-type and p-type elements).

3. Flexible: small size, lightweight and best suited for powering mobile systems and portable devices such as smart phone and personal computer.
4. No scale merit: however little in amount of heat, it will be directly converted into electricity.

In addition to the several advantages of thermoelectric mentioned above, note that if the power of sunshine is insufficient then the thermoelectric is more reliable for energy generation.

1.1. Thermoelectric phenomena

Thermoelectric is a physical phenomenon in science related to the production of electrical potential from the temperature gradient and vice versa. The thermoelectricity era began in 1821 after Thomas Johann Seebeck discovered the deflection of compass needle if placed near the closed-loop circuit made of two different metals with the junction maintained at different temperature. Seebeck erroneously assumed that this was a thermomagnetic effect. The development of thermoelectricity continued with the finding of Jean Charles Anthanase Peltier in 1834 who observed the opposite effect by passing a current through a series of conductor. However, Peltier did not relate his discovery to the one made by Seebeck 12 years earlier. In 1851, William Thomson (Lord Kelvin) found in the homogeneous conductor will either absorb or reject heat resulting from the flow of an electrical current in the present of a temperature gradient, as so called Thomson effect [4].

In the following, these phenomena encompass three separately identified effects: the Seebeck effect (1821), Peltier effect (1834) and Thomson effect (1851) in the term of Kelvin relationship will be introduced.

1.1.1. Seebeck effect

. The Seebeck effect involves the generation of voltage in the present of temperature difference in a device that consist of two different conducting materials [5]. If the pair is connected through an electrical circuit, direct current (DC) flows through that circuit. Fig. 1-2 shows in detail how the Seebeck effect works. In an open circuit (Fig. 2a), when 2 conducting materials A and B are kept across different temperature (ΔT) at 2 junctions (a and b), the temperature gradient is present and the voltage will be generated between the ends c and d (ΔV). If the open ends c and d are connected, electric current will generated and flow along the loop (Fig. 2b), which can be expressed as follows:

$$E = S_{AB} \nabla T$$

$$-\frac{dv}{dx} = S_{AB} \frac{dT}{dx} \quad \text{------}\rightarrow \quad S_{AB} = -\frac{dV}{dT} \tag{1.1}$$

Where E is electric field (Vm^{-1}), S_A and S_B are the absolute Seebeck coefficient of conductor A and conductor B meanwhile S_{AB} is the relative Seebeck coefficient of the AB circuits in volts per degree temperature difference($\mu V / K$).

The Seebeck coefficient could be positive or negative corresponding to a p-type and n-type material respectively. When heat is applied at one of the junction (hot side), the majority charge carriers in the materials (holes or electrons) have higher energies and velocities than charge carriers at the other junction (cold side), as a result the charge carriers diffuse from the hot side to the cold side, leaving their oppositely charge carriers at the hot side and generate a thermoelectric voltage. This voltage develops and opposing electric charge. The Seebeck coefficient is positive when the direction of thermal current is the same as the direction of electric current

and the Seebeck is negative when the direction of thermal current is opposite as the direction of electric current [6-8].

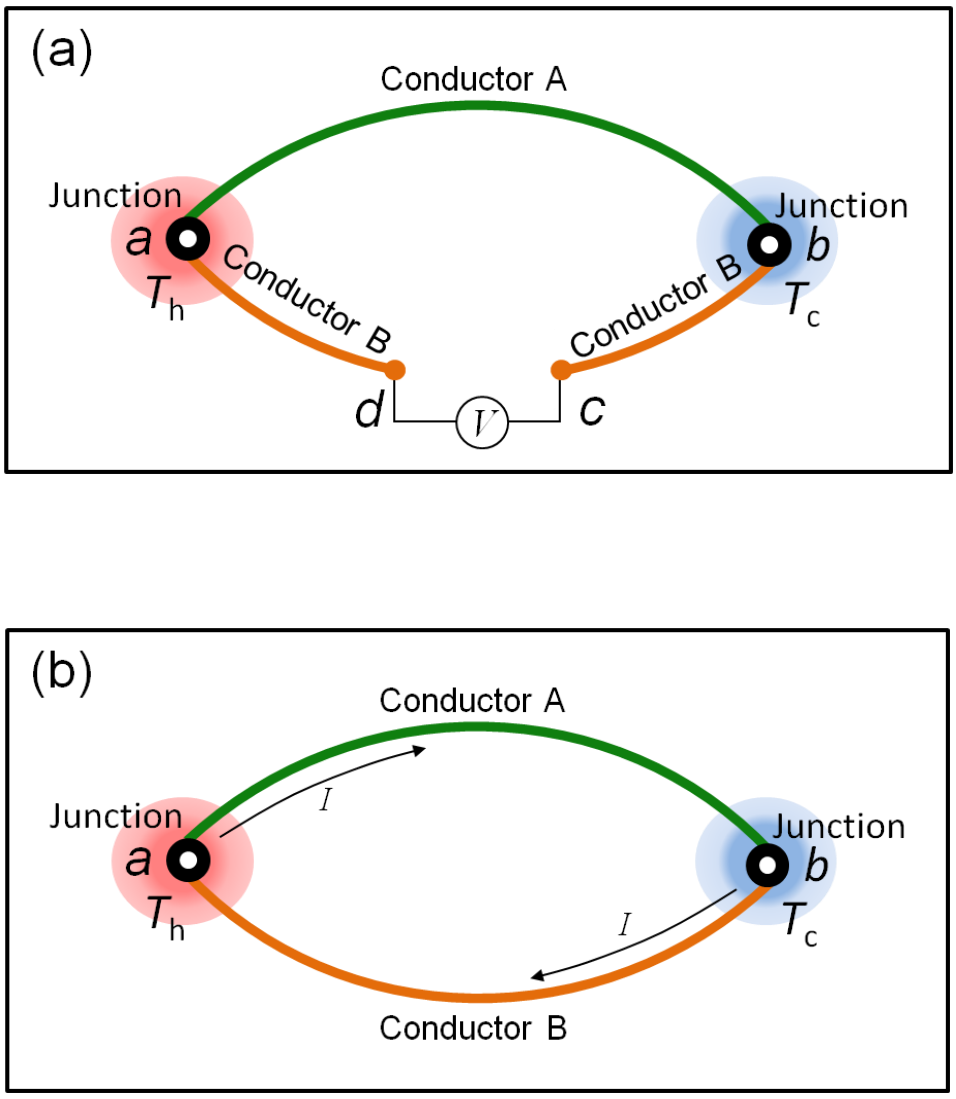

Fig. 1-2. Schematic illustration of the Seebeck effect. (a) Open circuit (b) Closed circuit.

1.1.2. Peltier effect

The Pertier effect is an inverse of Seebeck coefficient, as shown in Fig. 1-3a [6]. When the temperature gradient across a device of two different conducting materials (A and B) is generated in the present of an electrical current, the electric current that flows around the circuit results heat absorption at one junction (b) and the rate of heating is dQ/dt. On the other junction (a), the heat is rejected and the cooling rate is $-dQ/dt$. If the direction of electric current is changed, the heat absorption or rejection at the two junctions will reverse. The amount of heat absorbed and rejected at a junction depends on the amount of current supplied (I), which can be expressed as follows:

$$\frac{dQ}{dt} = \prod_{AB} \cdot I \tag{1-2}$$

Where $\prod_{AB}$ is the Peltier coefficient of A-B circuit which has a unit of Watt/A or in Volts.

The Pertier coefficient is positive when the electrical current flows in the same direction as the thermal current. If the electrical current flows in the opposite direction as the thermal current, the Peltier coefficient is negative. In other words, p-type materials will have positive Peltier coefficient and n-type material will have negative Peltier coefficient.

1.1.3. Thomson effect

The Thomson effect describes the rate of heating or cooling (dQ/dt) of a single current-carrying conductor (I) resulted along a portion of dx with a temperature gradient (dT/dx) as shown in Fig. 1-3 b [6]. Unlike the Peltier effect, Thomson effect only occurs along single material. The Thomson coefficient (μ_{JT}) can be expressed as follows:

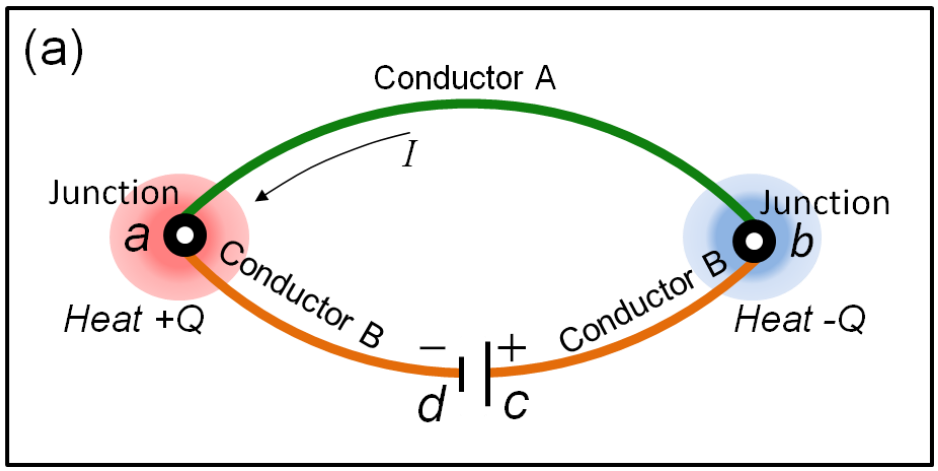

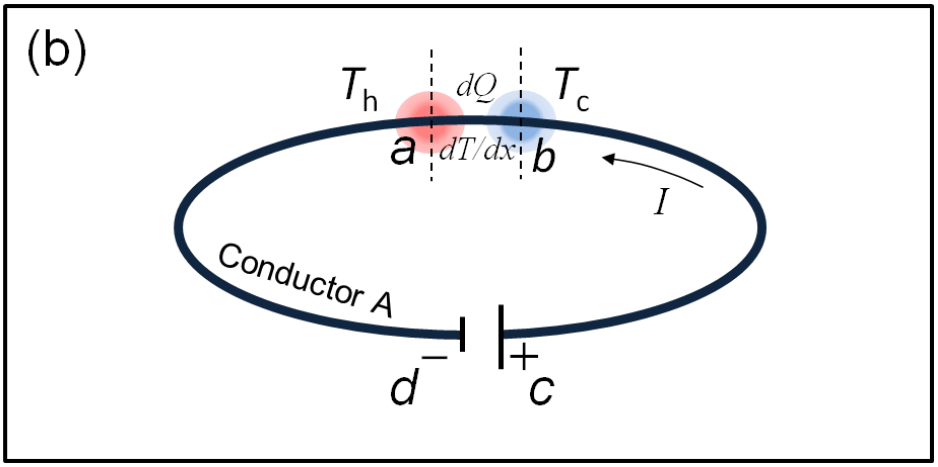

Fig. 1-3 (a) Pertier effect (b) Thomson effect.

$$\frac{dQ}{dt} = \mu_{JT} \cdot I \cdot \frac{dT}{dx}$$

(1-3)

The unit of Thomson coefficient is the same with unit of Seebeck coefficient, μV/K. Thomson coefficient is positive when the current flows from the hot side to the cold side and the heat is released. On the other hand of a reversed current, μ_{JT} is negative and the heat is absorbed.

1.2. Dimensionless figure of merit (*ZT*) and energy conversion efficiency

The potential of a material for thermoelectric application is evaluated by a measure of the figure of merits, *ZT*.

$$ZT = \frac{S^2\sigma}{\kappa}T \qquad (1\text{-}4)$$

where S, σ and κ are Seebeck coefficient, electrical conductivity and thermal conductivity, respectively, at a given absolute temperature, T. Achieving a material with a high *ZT* value, three parameters (S, σ and κ) should be controlled where S and σ should be large simultaneously while κ should be very low [9]. κ is the sum of electrical thermal conductivity (κ_e) and lattice thermal conductivity (κ_l), $\kappa = \kappa_e + \kappa_l$. However, these three parameters are related to one another and have dependence on the carrier concentration (n), as shown in Fig.1-4a. The increase in carrier concentration will lead to an increase in electrical conductivity and decrease in Seebeck coefficient simultaneously.

The dependence of *ZT* value on the carrier concentration has been proposed for a standard band type semi conductor and can be expresses as follows [10.11]:

$$Z = \frac{S^2\sigma}{\kappa} \propto \frac{m^{*3/2} \cdot \mu}{\kappa} \quad (1\text{-}5)$$

and

$$\sigma = n.e.\mu \quad (1\text{–}6)$$

where m^* is the effective mass of carriers, e is electron charge and μ is carrier mobility. These parameters are also has the role for the increase in *ZT* as follows:

1. The increase in effective mass of carriers (m^*) will give rise to a larger Seebeck coefficient (S).
2. Hall mobility of carrier should be optimized to obtain a large electrical conductivity (σ).
3. On the other hands, keep maintaining low thermal conductivity is crucial to achieve the optimal *ZT* value.

Finding a material which exhibits a high *ZT* value is always be a challenge for thermoelectric researcher because *ZT* is a function of energy conversion efficiency and the maximum efficiency ($\eta_{\max}$) can be defined as follows [12],

$$\eta_{\max} = \frac{T_H - T_C}{T_H} - \frac{\sqrt{1+ZT}-1}{\sqrt{1+ZT}+\frac{T_c}{T_H}} \quad (1\text{-}7)$$

where T_H is the temperature at the hot junction and T_C is the temperature at the surface being cooled. High *ZT* value will contribute to larger energy conversion efficiency as illustrated in Fig. 1-4b.

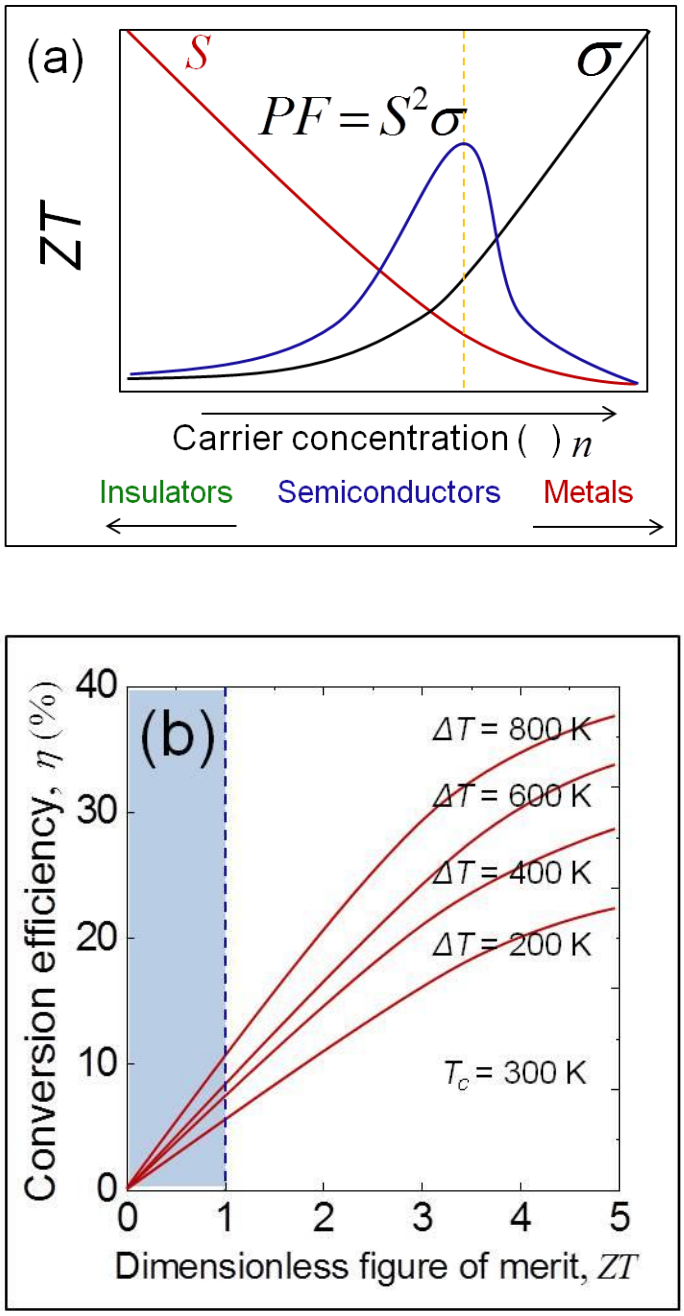

Fig. 1-4. (a) The relationship of Seebeck coefficient, S, electrical conductivity, σ and power factor, $S^2\sigma$ on the carrier concentration, n (b) The conversion efficiency as a function of dimensionless figure of merit, *ZT.*

1.3. Thermoelectric materials

This is a great challenge in finding a high performance thermoelectric material because since the discovery of thermoelectricity there has not been much development in practical application due to poor material's performance. Various ways have been cultivated by researcher to optimize the performance of thermoelectric materials. Many classes of promising novel material has been investigated, some methods are modified to understand their behavior and great effort are performed to improve their thermoelectric properties. Recently, many new materials have been discovered and studied by thermoelectric researcher, thus in this session will be discussed in three categories of inter metallic, oxide and misfit layer compound.

1.3.1. Intermetallic

The initial researchers were focused on the binary intermetallic semiconductor system and its alloys that have high electrical conductivity. However, it was found that the Seebeck coefficient in metal was low. Moreover, a high electronic thermal conductivity due to the high electrical conductivity which is related by Wiedemann-Franz law results in an increase in total thermal conductivity.

Due to the strong dependency of thermoelectric properties on temperature, the well-established thermoelectric material, bismuth telluride (Bi_2Te_3) has a limitation in the practical operation. It was found to be suitable for operation at a temperature ranges between 300-500 K [13.14]

Recent approaches the researchers focused on the ternary and quaternary chalcogenides containing heavy atoms with low dimensional or isotropic complex structures to get the merit of the large carrier effective mass and low lattice thermal conductivity [15.16]. The germanium based TAGS (Te-Ag-Ge-Sb) has considered to be more efficient but its high sublimation rate and low temperature phase transition have found little use

[17].

The concept of introducing “guest” atoms into the void in the skutterudites (partially filled) has greatly reduced the lattice thermal conductivity of these compounds and resulted in improvement in TE properties. The main aim in investigating partially filled skutterudites is realizing an optimum carrier concentration (electron) while reducing the thermal conductivity, thereby maximizing *ZT* value [18.19].

However, due to the strong dependency of thermoelectric properties on temperature, intermetallic materials have limited capability in practical application due to oxidation. Moreover, these materials generally consist of hazardous elements which can be harmful to the environment.

1.3.2. Oxide.

Oxides have received little attention because of their strong ionic character and low carrier mobility due to localized electron caused by a narrow conduction band-width arising from weak orbital overlap. However, the discovery of good thermoelectric properties of p-type $NaCo_2O_4$ has inspired thermoelectric researchers to explore the potential of oxide as a promising thermoelectric material [20.21]. Moreover, there are many oxides with metal atom are stable at elevated temperature and show electrical properties ranging from insulating to superconducting. Recently, the current studies are focused on Co-based layer structure, crystallizing in misfit (lattice mismatch) layer compound and constructing 3D superlattice base nanocubes [22-24]. These approaches are carried out to get the advantages on low thermal conductivity in oxides materials.

1.3.3. Misfit layer compound

Crystal symmetry and materials engineering approach in realizing good thermoelectric material receive the most attention from TE researchers. Understanding the superior properties of material and selecting the

strategies to improve its shortcomings are a huge challenge because in complex materials there are many possible degrees of freedom.

Slack has described the chemical characteristic for good candidates TE materials should be narrow bandgap semiconductor with high mobility of carriers. In agreement with Slack, Mahan also added the typically narrow bandgap semiconductor posses $E_g \approx 0.25$ eV and the mobility of carriers, $\mu \approx 2000$ cm^2/Vs at 300 K, while the lattice thermal conductivity must be minimized. Since then, researchers followed the concept offered by Slack to search TE materials with the electrical properties of a crystalline material and the thermal properties of a glass-like material or amorphous, known as phonon glass electron-crystal (PGEC) [25.26].

The dimensional approach (1D and 2D) proposed by Hicks and Dresselhaus plays an important role in the electronic transport for a given materials even it can change the system from metallic to semiconducting behavior [27-29]. The low dimensional character of thin film structure (2D) had given a significant improvement for the enhancement of *ZT* value in Bi_2Te_3/Sb_2Te_3 superlattice. The enhancement is attributed to a creating a nano-structured that is efficient for thermal insulation while maintaining good electrical properties [30].

Recently, a novel material of dichalcogenide misfit layer compounds $(MS)_x(TiS_2)_2$ (M=Pb,Sn,Bi;1.18<x<1.2) proposed by Koumoto had attracted a lot of attention because in addition to be a promising, this material is eco-friendly which naturally abundant, non toxic and cost effective [31-33]. Dichalcogenides misfit layer compounds posses a composite structure made up of two sub lattices of MS and TS_2 with different chemical composition, unit cell and space group. The misfit or incommensurate comes from periods along the direction of b axis so that the geometries are different and lack of three dimensional periodicity.

This structure has been able to improve the thermoelectric performance of $(MS)_x(TiS_2)_2$ misfit layer sulfide by taking the advantage in reducing the thermal conductivity. Figure 1-5 shows the ZT value as a

function of temperature of some thermoelectric materials known nowadays.

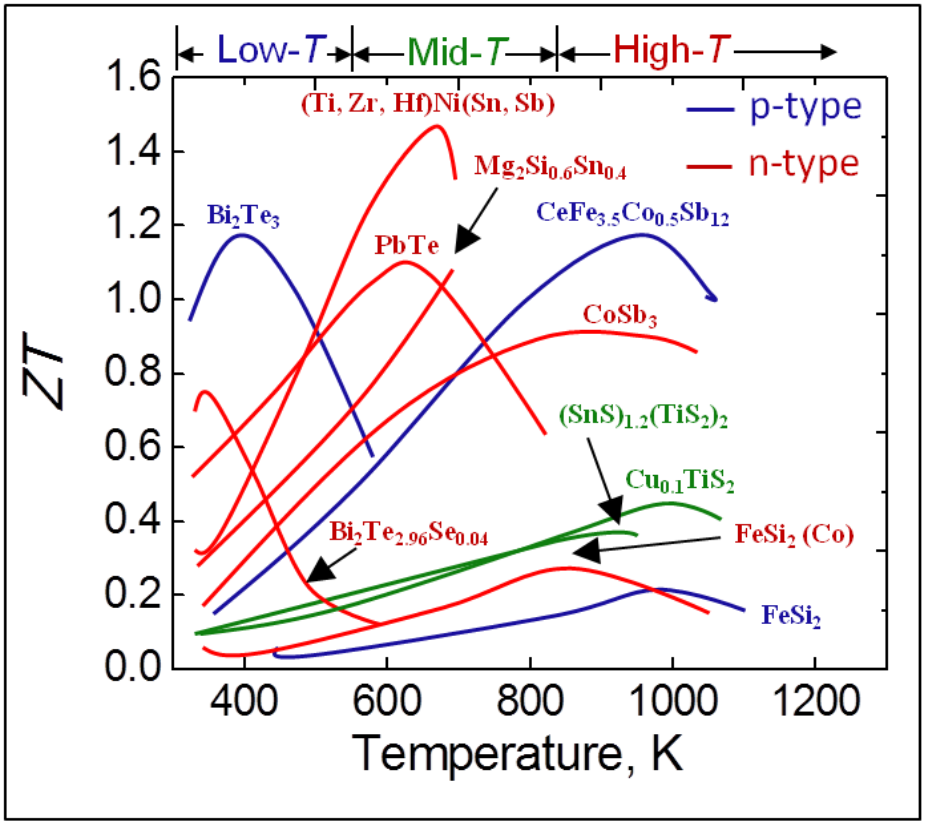

Fig 1-5. The *ZT* value dependence on temperature of thermoelectric materials [R. Funahashi, AIST].

1.4. Aim and objectives

It have been reported that the series of transition-metal dichalcogenides $(MS)_x(TiS_2)_2$ misfit layer sulfides (M=Pb,Sn,Bi;1.18<x<1.2) could become a promising thermoelectric materials. These compounds are constructed by two layers TiS_2 and one layer metal sulfide (PbS, SnS, BiS). TiS_2 has shown its potential as a promising thermoelectric material through its high power factor $(S^2\sigma)$ at room temperature. However, its TE performance is limited by its high thermal conductivity, so that the *ZT* value is not optimal. The intercalation of MS layers had become an effective way of reducing the thermal conductivity. However, reducing the thermal conductivity in this manner led to an increase in carrier concentration due to electron transfer from MS layers to the TiS_2 layers, thereby increasing the electrical conductivity and electronic thermal conductivity. As a result of this phenomenon, the Seebeck coefficient decreases and the power factor cannot be optimized; moreover, the total thermal conductivity is not sufficiently suppressed.

In this study, we are focusing in the $(BiS)_{1.2}(TiS_2)_2$ misfit layer sulfide because among the three metal sulfide, BiS most effectively reduced the thermal conductivity, especially the lowest lattice thermal conductivity. The formation of disorder structure and the planar stacking faults in the $(BiS)_{1.2}(TiS_2)_2$ results in the low lattice thermal conductivity. Moreover, the mobility of carriers in this compound did not change.

The aim of this study is to enhance the thermoelectric properties of $(BiS)_{1.2}(TiS_2)_2$ misfit layer sulfide, particularly improving the electrical properties by taking the merits of very low lattice thermal conductivity and no change in their carrier mobility. The strategy to enhance the electrical properties is by doping low valency dopants, as so called the modulation or selective doping. To achieve this challenging goal, a number of key objective have been defined as follows:

1. To determine which sites in each layer will be doped by the dopants.
2. To search appropriate dopants which are doped into the host atom in the TiS_2 layer or in the BiS layer.
3. To verify most favorable doping amount (wt %) of each dopant.

1.5. $(BiS)_{1.2}(TiS_2)_2$ misfit layer sulfides

1.5.1. Crystal structure

Misfit layer chalcogenides $(MX)_p(TX_2)_n$ ($1.08<p<1.23$; n=1-3) have layer structure which constructed by alternately stacking of double layer MX (M= Sn, Pb, Sb, Bi, rare earth metals; X= S, Se) and TX_2 slabs(T= Ti, V, Nb, Ta, Cr). The MX slab has a pseudo-tetragonal symmetry and consist of distorted rock-salt structure [34]. The TX_2 slab in which the transition metal T is surrounded by chalcogen atoms, either in octahedral coordination (T= Ti, V, Cr) or in trigonal prismatic coordination (T= Nb, Ta). Misfit (incommensurate) behavior arises from the non-coincidence of periodicities between the two distinct sets, along the crystallographic direction at least one direction, which means that bTM ≠ $b(TX_2)$ while the periodicities along a and c directions are identical; c was selected as the stacking direction. The ratio of MX to $(TX_2)_n$, is determined by the ratio of the b axes of the two sub systems and the length ratio is found to vary between 1.56 and 1.85 [35]. The simple diagram is illustrated in Fig. 1-6.

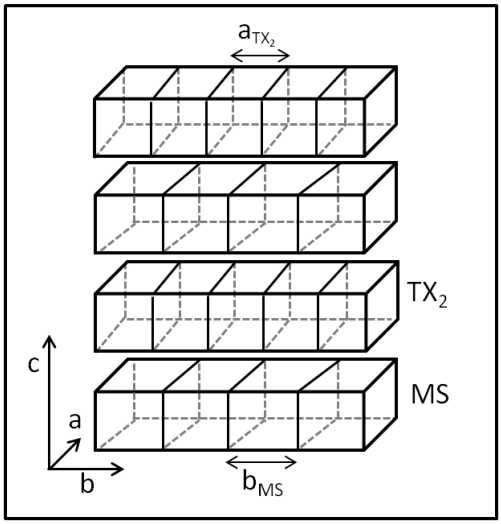

Fig 1-6. The structure of $(MS)_n$ (TX_2) given as the building units MS and TX_2.

$(BiS)_{1.2}(TiS_2)_2$ is one of the misfit layer chalcogenide group which have been reported as a promising thermoelectric material [2.31]. It composed of two layers TiS_2 and one layer BiS with a regular arrangement where TiS_2 layer has a role as an electron transmitting and BiS layer as a phonon blocking, as shown in Fig. 1-7.

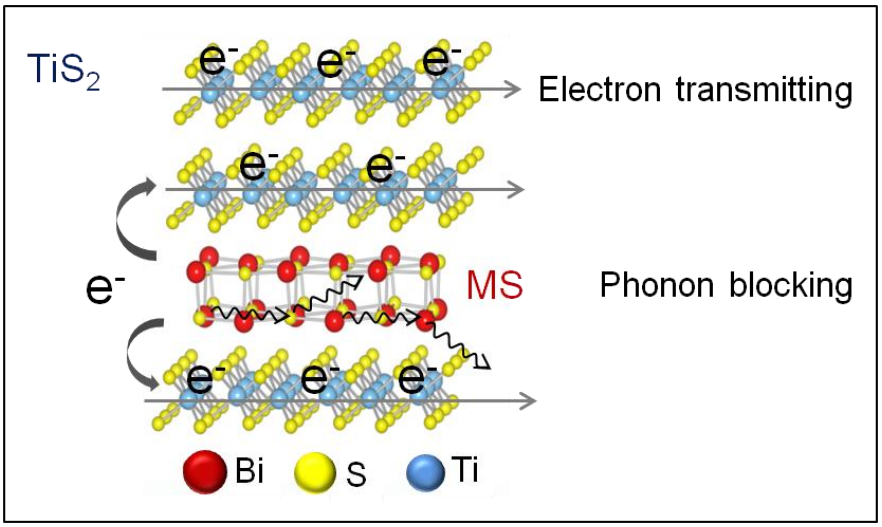

Fig 1-7. The structure of $(BiS)_{1.2}$ $(TiS_2)_2$ misfit layer sulfide.

Titanium disulfide TiS_2 belongs to a wide group of *d*-metal dichalcogenides MX_2 layer structure (M=metal and X= S or Se). The structure of TiS_2 consists of packed S-Ti-S molecular layers; inside the layers are bonded by strong covalent interaction and between the layers are linked by weak van der Waals interaction. In the van der Waals gap, some Lewis bases (organic or inorganic) can be intercalated [36.37].

TiS_2 has two polytypes; 1T and 2H. 1T is the most stable polytypes with P3m1 symmetry group where Ti atom is surrounded by sulfur atoms in octahedral coordination. 2H is the metastable polytypes with C6/mmc symmetry group that consist of conjugated trigonal prisms as shown in Fig. 1-8.

TiS_2 crystal is a semimetal due to the overlap between the S p and Ti d bands near the Fermi level with the band gap energy is 1.65 eV. However, the monolayer of TiS_2 falls into semiconductor with the band gap energy is 0.2-0.3 eV. The transition from semiconductor to metal-like state occurs for a plate of more than ten molecular layers.

1.5.2. Previous research on $(BiS)_{1.2}(TiS_2)_2$ misfit layer sulfide

A series of study on the TiS_2 for thermoelectric material has become a topic of interest for thermoelectric researchers in recent years. Its promising electrical properties have driven a comprehensive study on how to optimize all thermoelectric parameters in TiS_2 compound. It has been reported by Imai that nearly stoichiometric TiS_2 posses a high power factor ($S^2\sigma$) at room temperature [38]. However, its TE performance is limited by its high thermal conductivity, so that the *ZT* value is not optimal. Since then, much research has focused on how to reduce high thermal conductivity without degrading high power factor.

Intercalation of BiS in the van der Waals gap between the TiS_2 layers forming $(BiS)_{1.2}(TiS_2)_2$ have effectively reduced thermal conductivity and even contributed to an ultralow lattice thermal conductivity at higher temperature [31.32]. The formations of large density planar interfaces, which are only a few unit cells apart, had caused the phonon confinement or phonon localization behavior. However, reducing the thermal conductivity in this manner does not increase the value of *ZT*; electron transfer from BiS layers to the TiS_2 layers increases the carrier concentration, thereby increasing the electrical conductivity and electronic thermal conductivity. As a result of this phenomenon, the Seebeck coefficient decreases and the power factor cannot be optimized; moreover, the total thermal conductivity is not sufficiently suppressed.

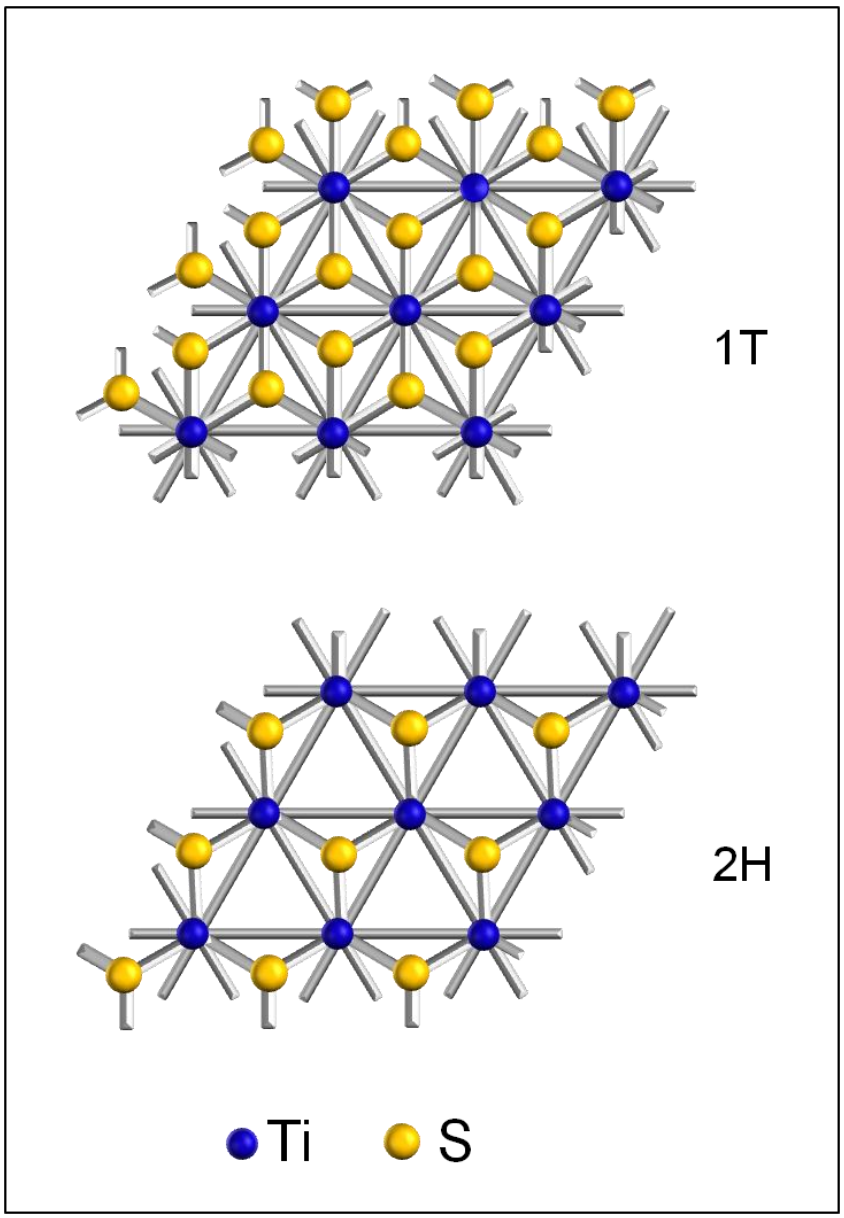

Fig 1-8. The structure of 1*T*- and 2*H*-TiS_2 phases molecular layer.

References

[1] G.A. Slack, New Materials and Performance Limits for Thermoelectric Cooling, in: D.M. Rowe, CRC Handbook of Thermoelectric, CRC Press: Boca Raton, FL, USA, (1995) pp.407–440.

[2] C.L. Wan, Y.F. Wang, N. Wang, Y.E. Putri, W. Norimatsu, M. Kusunoki, K. Koumoto, Layered Structure Metal Sulfides as Novel thermoelectric materials, in: D.M. Rowe, Modules, System and Application in Thermoelectric, CRC Press: Boca Raton, FL, USA, 2012, p.4.1–4.11.

[3] G. D. Mahan and J. 0. Sofo, Appl. Phys. Sci. 93 (1996) 7436-7439.

[4] A. F. Ioffe, “Semiconductor Thermoelements and Thermoelectric Cooling”, Infosearch Limited, London, (1957).

[5] Francis J. DiSalvo, Science 285 (1999) 703-706.

[6] Robert R.B., Nature 265 (1977) 226–227.

[7] L.I. Anatychuk, Physics of Thermoelectricity, Institute of Thermoelectricity, Ukraine (1998) 176-177.

[8] T. M. Tritt, “Thermoelectric Materials: Principles, Structure, Properties, and Applications”, Encyclopedia of Materials Science and Technology, (2002) 1-11.

[9] D. M. Rowe, “Introduction”, CRC Handbook of Thermoelectrics, CRC Press LLC, Boca Raton, (1995) 1-6.

[10] H. J. Goldsmid, Electronic Refrigeration,Pion,London (1986) 36-45.

[11] G. Jeffry Snyder, T. Caillat and J.P.Fleurial, Phys. Rev. B 62 (2001) 10185.

[12] H. J. Goldsmid, “Conversion Efficiency and Figure-of-Merit”, CRC Handbook of Thermoelectrics edited by D. M. Rowe, CRC Press LLC, Boca Raton, (1995) 19-25.

[13] C.B. Satterthwaite and R.W. Ure, Jr., Phys. Rev. 108, (1957) 1164-1170.

[14] H. J. Goldsmid, A. R. Sheard, and D. A. Wright, J. Appl. Phys. 9 (1958) 365-370.

[15] R. Venkatasubramanian, E. Siivola, T. Colpitts, and B. O'Quinn, Nature 413 (2001) 597.

[16] Terry M.Tritt and M.A. Subramanian, MRS BULLETIN 31 (2006) 118-229.

[17] E. Skrabeck and D.S. Trimmer, in CRC Handbook of Thermoelectric, CRC Press: Boca Raton, FL, USA, (1995) pp.267-275.

[18] G.S. Nolas, D.T. Morelli and T.M. Tritt, Annu. Rev. Mater. Sci. 29 (1999) 89-116.

[19] Terry M. Tritt, Science 272 (1996) 1276-1277.

[20] H. Ohta, SungWng Kim, Yoriko Mune, Teruyasu Mizoguchi, Kenji Nomura, Shingo Ohta, Takashi Nomura, Yuki Nakanishi, Yuichi Ikuhara, Masahiro Hirano, Hideo Hosono and Kunihito Koumoto., Nature Mater. 6 (2007) 129-134.

[21] Shingo Ohta, Takashi Nomura, Hiromichi ohta and Kunihito Koumoto, J. Appl. Phys. 97 92005) 034106.

[22] Terayuki Itoh and Ichiro Terasaki, Jpn. J. Appl. Phys 39 (2000) 6658-6660.

[23] I. Terasaki, Y. Sagano and K. Uchinokura, Pyhs. Rev. B. 56 (1997) R12685.

[24] Lambert, D. Pelloquin, and A. Maignan, Phys. Rev. B. 64 (2001) 172101-172104.

[25] George S. Nolas, Glen A. Slack, Sandra B. Schujman, Semiconductor and Semimetal, 69 (2001) 255-300.

[26] Donald T. Morelli and Glen A. Slack, High Lattice Thermal Conductivity Solids in High Thermal Conductivity Materials, Springer Science, Bisnis Media Inc, USA (2006) 37-64.

[27] Kunihito Koumoto, Ichiro Terasaki and Ryoji Funahashi, MRS Bull.,

31 (2006) 206-209.

[28] M. Ahrensa, R. Merkleb, B Rahmatic, J. Maier, Phisica B, 393 2007) 239-248.

[29] S. Ohta, H. Ohta and K. Koumoto, J. Ceram. Soc. Jpn. 114 (2006) 102.

[30] A.J. Minnich, M. S. Dresselhaus, Z. F. Ren and G. Chen., Energy Environ. Sci.466 (2009) 2-466–479.

[31] Chunlei Wan, Yifeng Wang, Ning Wang and Kunihito Koumoto, Materials 2010, 3:2606–2617.

[32] Chunlei Wan et al, J. Electron Mater 49. 5 (2011) 1271–1280.

[33] Chunlei Wan, Yifeng Wang, Wataru Norimatsu, Michiko Kusunoki and Kunihito Koumoto, Appl. Phys. Lett. 2012, 100:101913-1-101913-4.

[34] J. Rouxel, A. Meerschaut, G.A. Wiegers, J. Alloys Compd. 229 (1995) 144–157.

[35] A. Meerschaut , R. Roesky, A. Lafond, C. Deudon, and J. Rouxel, J. Alloys Comp. 219 (1995) 157-160.

[36] V. V. Ivanovskaya, G. Seifert and A. L. Ivanovskii, Semiconductors 39 (2005) 1058–1065.

[37] Mitsuko Onoda, Masanobu Saeki and Isao Kawada, Physica 105B (1981) 200-204.

[38] H. Imai, Y. Shimakawa,Y. Kubo, *Phys. Rev.* B 64 (2001) 241104.

Chapter II

Measurements and Characterizations of Thermoelectric Material

Thermoelectric properties are evaluated based on three parameters: the Seebeck coefficient, electrical conductivity and thermal conductivity. These parameters were measured to clarify the potential of misfit layer sulfide as a novel thermoelectric material [1]. Therefore, thermoelectric properties measurements were conducted in this study are electrical conductivity, Seebeck coefficient, thermal diffusivity, specific heat capacity, sound velocity, Hall mobility and carrier concentration. The structural analysis and morphology observation are also carried out as SEM and TEM to clarify the crystal structure, phase composition, shape, size and the layer orientation of the samples. The other measurement is X-ray photo spectroscopy (XPS) to determine the ionic state of each dopant in the samples.

In this chapter, the relevant measurement of thermoelectric properties, structural analysis, morphology observation including methods of measurement will be discussed in detail.

2.1. Structural analysis and morphology observation.

The structural analysis was based on the X-ray diffraction (XRD) measurement. The measurement was conducted for powder and pellet samples. The powder samples were ground and sieved (grain size is less than 10 μm), and then were pressed into the glass sample holder with another piece of glass sample holder gently. The pellet samples were cut and polished with sandpaper smoothly. The measurement for pellet samples were conducted in the direction perpendicular with the pressure applied during sintering process. The XRD measurement is carried out on a 2.5 kW (50 KV, 50 mA) Rint2100 diffractometer (Rigaku Co. Japan). The main parameter of measurement condition was set as 30 kV, 40 mA and the X-ray source is copper (Cu K α : λ = 1.5418 Å).

The morphology observation was carried out by SEM and TEM. SEM observation is aimed to determine shape and size of the powder samples

and layer orientation in the pellet samples. The powder samples were observed from the fine power after sintering. The pellet samples were observed in direction perpendicular with the pressure applied during sintering. TEM observation was carried out in for the pellet samples to examine the layer structure in the samples. The direction perpendicular with the pressure applied during sintering. The pellet was polished smoothly using sandpaper into a thin pellet (thickness ~ 80 μm). The final form such as wafer as follows: 2 layers silicon glass, 1 layer thin sample and 2 layers silicon glass. The surface of the wafer sample which will be observed was polished smoothly and shiny with diamond paste (diamond paste based water solution 1 μm). The molybdenum ring was posted carefully on the shiny surface where the thin sample was exactly in the middle of the ring. The final shape of the wafer sample is shown in Fig. 2-1.

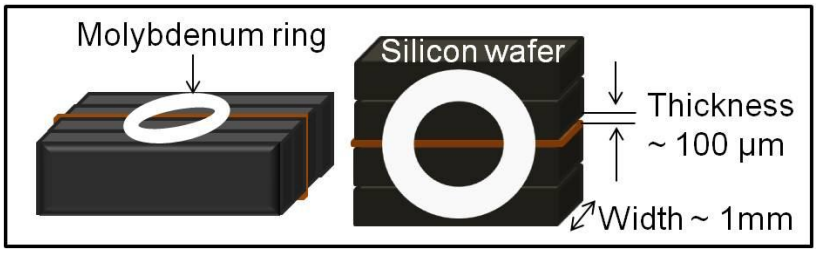

Fig. 2-2. The final shape of the wafer sample for TEM observation.

2.2. Ionic state analysis

XPS measurement was performed to analyze the ionic state of all dopants. The bulk samples were cut and the surface perpendicular with the pressure applied during sintering polished smoothly with diamond paste (diamond paste based water solution 1 μm). The glossy surface was wiped with ethanol and dried with a dryer, and then sample was placed in a holder. The measurement conditions were set as; 10 kV, 10 mA with and

the X-ray source is aluminum (Al K α : λ = 8.3386 Å).

2.3. Electrical conductivity

Electrical conductivity, σ is a measure how well a material accommodates the transport of an electric charge [2]. Its SI derived unit is the Siemens per meter ($A^2s^3m^{-3}kg^{-1}$) (named after Werner von Siemens) or, more simply, Sm^{-1} and is defined as the reciprocal value of the resistance ρ as follows:

$$\sigma = \frac{1}{\rho} \tag{2-1}$$

while

$$\rho = R\frac{A}{l} \tag{2-2}$$

and

$$R = \frac{U}{I} \tag{2-3}$$

so

$$\sigma = \frac{1}{R\frac{A}{l}} = \frac{1}{\left(\frac{U}{I}\right).\left(\frac{A}{l}\right)} = \frac{I/A}{U/l} = \frac{J}{E} \tag{2-4}$$

where R is the electrical resistance (ohms, Ω), A is the cross section area of the specimen (square meters, m^2), is the distance between the 2 probes (meters, m), U is the voltage difference across the probes (volts, V), I is the current (Ampere, A), J is the current density (Ampere per square meter, A/m^2) and E is the electrical field (volts per meter, V/m) respectively [3].

In the misfit layer sulfide, a negative value of Seebeck coefficient shows that the main carriers is electron and the density of electrons, n_e is extremely larger than that of the holes, n_p, so

$$I = -n_e q v_d \text{ x } 1 \text{ x } s \Rightarrow J \tag{2-5}$$

and

$$v_d = \mu|E| \quad (2\text{-}6)$$

thus

$$\sigma = n_e q \mu \quad (2\text{-}7)$$

Where n_e is the carrier concentration (cm^{-3}), q is the electron charge, v_d is the drift velocity and μ is the carrier mobility (m^2/Vs).

The following equation is referred to the band theory where n_e can be represented as follows:

$$n_e = \int_{E_c}^{E_{max}} D(E) f(E) dE \quad (2\text{-}8)$$

where E_{max} and E_c are the energy level of the conduction band top and bottom, $D(E)$ is the density of states and $f(E)$ is the function of carrier distribution. For an *n*-type misfit layer sulfide degenerate semi conductor which has large carrier concentrations n_e ~ 10^{21}, n_e is evaluated with the equation below.

$$n_e = \frac{4\pi(2m^*)^{3/2}}{h} \int_{E_c}^{\infty} \frac{(E-E_c)^{1/2}}{1+\exp\left[\frac{E-E_F}{k_0 T}\right]} dE = \frac{4\pi(2m^*)^{3/2}}{h^3} F_{1/2}(\xi) \quad (2\text{-}9)$$

where

$$F_{1/2}(\xi) = \int_0^{\infty} \frac{x^{1/2}}{1+e^{x-\xi}} dx \quad (2\text{-}10)$$

and

$$\xi = \frac{E_F - E_c}{k_o T} \quad (2\text{-}11)$$

Fermi level is affected by the doping density, temperature and material compositions whereas the carrier concentration is determined by material, doping method and temperature. The carrier concentration can be determined experimentally by using Hall effects measurement as well as the type of carrier and the mobility of carrier simultaneously.

The experimental setting of electrical conductivity is simply illustrated

in Fig 2-2, where the Seebeck coefficient can be measured simultaneously.

The measurement of electrical conductivity was carried out by using 4 probe methods [4-6]. In this method the measurement technique used two outer probes and 2 inner probes; outer probe is used to introduce a fixed current into the sample while inner probe measured the voltage produced. The advantages of this technique are:

1. The separate probe for current and voltage will eliminate the electrical contact resistance because negligible current pass through the voltage probes.
2. If the voltage probes are place close each other and far from the current probes, the uniform current flows between the voltage probes can be attained.

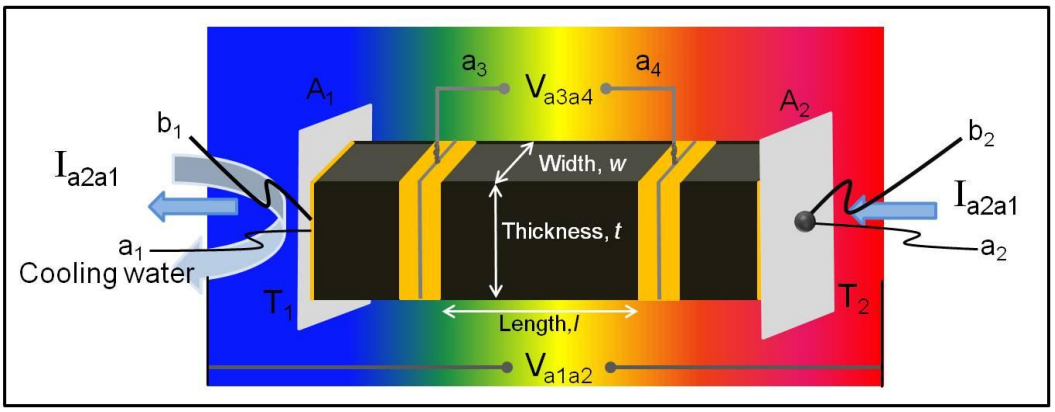

Fig. 2-2. Schematic illustration of experimental setting for electrical conductivity (a DC four probe method) and Seebeck coefficient (a steady state method) measurement.

2.4. Seebeeck Coefficient

TiS_2-based misfit layer sulfides possess high carrier concentration, so that the distribution of carrier obeys the Fermi distribution function. Culler and Mott derive the Seebeck coefficient in this formalism

$$S = \frac{k_B}{q}\frac{1}{\sigma}\int_0^\infty \sigma(E)\left(\frac{E-E_F}{k_BT}\right)\left(\frac{\delta f_0(E)}{dE}\right)dE \quad (2\text{-}12)$$

In the system in which the Fermi statistics are degenerate such as metal and degenerately doped semiconductor, the Seebeck coefficient and the Fermi integral can be define as:

$$S = -\frac{k_B}{e}\left[\frac{(r+2)F_{r+1}(\xi)}{(r+1)F_r(\xi)} - \xi\right] \quad (2\text{-}13)$$

$$F_n(\xi) = \int_0^\infty \frac{x^n}{1+e^{x-\xi}}dx \quad (2\text{-}14)$$

where k_B is the Boltzman constant (1.381x10^{-23} J/K) and e is the electric charge (1.602x10^{-19} C).

Fig. 2-2 also includes the schematic illustration of seebeck coefficient measurement. The measurement is carried out in the steady state method which is defined as:

$$S_{sample} = S_{(sample-Pt)} - S_{Pt} \quad (2\text{-}15)$$

where S_{sample} is the thermo power of the sample, $S_{(sample-Pt)}$ is the thermo power of the circuit made of sample and Pt probe and S_{Pt} is the thermo power of the Pt probe, respectively.

In the measurement system, the value of S_{Pt} at varies temperature are already known whereas the S_{sample} can be obtained as describe in equation 2.13. Subsequently, $S_{(sample-Pt)}$ value can be obtained from the voltage and temperature differences across the cold and hot end. Therefore, the observed value of $S_{(sample-Pt)}$ can be describe as

$$S_{(sample-Pt)} = \frac{-V}{T_H - T_c} \quad (2\text{-}16)$$

In the measurement system, the practical value was sampled 5 times within a temperature difference range of 2~15 K, then a statistic value of the sample was calculated.

The sample typically rectangular with the dimension is about 2 mm x 2 mm x 6 mm. The surfaces of the sample in contact with Pt probe should be sputtered with a thin Au for a better contact between the sample and the 4 Pt probes.

2.5. Thermal conductivity

Thermal conductivity κ is a measure of the ability of a material to transfer heat [10]. The tensor of thermal conductivity in the thermoelectric materials can be represented as the sum of thermal conductivity of current carrier, $\kappa_{electronic}(\kappa_e)$ and the contribution of phonon transport or lattice thermal conductivity, $\kappa_{lattice}(\kappa_l)$.

$$\kappa_{total} = \kappa_e + \kappa_l \tag{2-17}$$

$\kappa_{electronic}$ can be expressed by the law of Wiedemann-Franz as follow:

$$\kappa_e = L_0 \cdot \sigma \cdot T \tag{2-18}$$

where L_o is the Lorentz number (2.44×10^{-8} $W\Omega K^{-2}$), σ is the electrical conductivity (Scm^{-1}) and T is temperature (K). The value of L_o depends on the energy spectrum model, scattering mechanism and the degree of degeneracy, thus define as:

$$L_o = \left(\frac{k_B^2}{e^2}\right)\left[\frac{s+3}{s+1}.\frac{F_{s+2}(\xi^*)}{F_s(\xi^*)} - \frac{(s+2)^2}{(s+1)^2}.\frac{F_{s+1}^2(\xi^*)}{F_s(\xi^*)}\right] \tag{2-19}$$

where F_s, F_{s+1}, F_{s+2}, are the Fermi integrals, s=0, for acoustic phonon scattering, s=1 for optic phonon scattering, s=2 for impurity ion scattering and ξ is chemical potential of current carriers ($\xi^* = \xi/k_BT$). With strong degeneracy,

$$L_o = \left(\frac{\pi^2}{3}\right)\left(\frac{k_B^2}{e^2}\right) \tag{2-20}$$

The Fermi integral value were obtain from the measured S from equation 2-13 and 2-14.

In the present experiment, the value of κ was obtained by using the following equation:

$$\kappa = \rho \cdot \alpha \cdot C_p \qquad (2\text{-}20)$$

Where ρ is the observed density of the sample (g/cm^3), α is the thermal diffusivity (cm^2/s) and C_p is the specific heat capacity (J/gK).

The observed density was simply calculated by using weight and volume, thermal diffusivity was measured with a laser flash method and C_p was determined by using a differential scanning calorimeter.

2.5.1. Thermal diffusivity

Laser flash method is the most popular method for measuring thermal conductivity in the solid [11]. The measurement used a pellet samples which were cut and polished into a square shape with the dimensions of ~ 1 mm (thickness) x ~ 6 mm (width), then one side of the surface was sprayed with liquid carbon (colloidal carbon in 44% in isopropyl alcohol) and dried. The surface of the sample with no carbon sprayed was subjected to a very short pulse of heat from a laser. The resulting temperature rise on the back surface of the sample is recorded by a chart recorder. The value of α can be expressed as:

$$a = 1.37 \frac{d^2}{\pi^2 t_{1/2}} \qquad (2\text{-}22)$$

where d is the thickness of the samples (mm) and $t_{1/2}$ is the half-time of the surface opposing the laser incidence direction to reach the maximum temperature increase ΔT_{max} after the absorption of the heat supplies from the laser source and ΔT_{max} can be expressed as

$$\Delta T_{max} = \frac{Q_L}{\rho C_p d} \quad (2\text{-}23)$$

Where Q_L is the heat of the sample absorbed from each laser pulse as shown in Fig. 2-3.

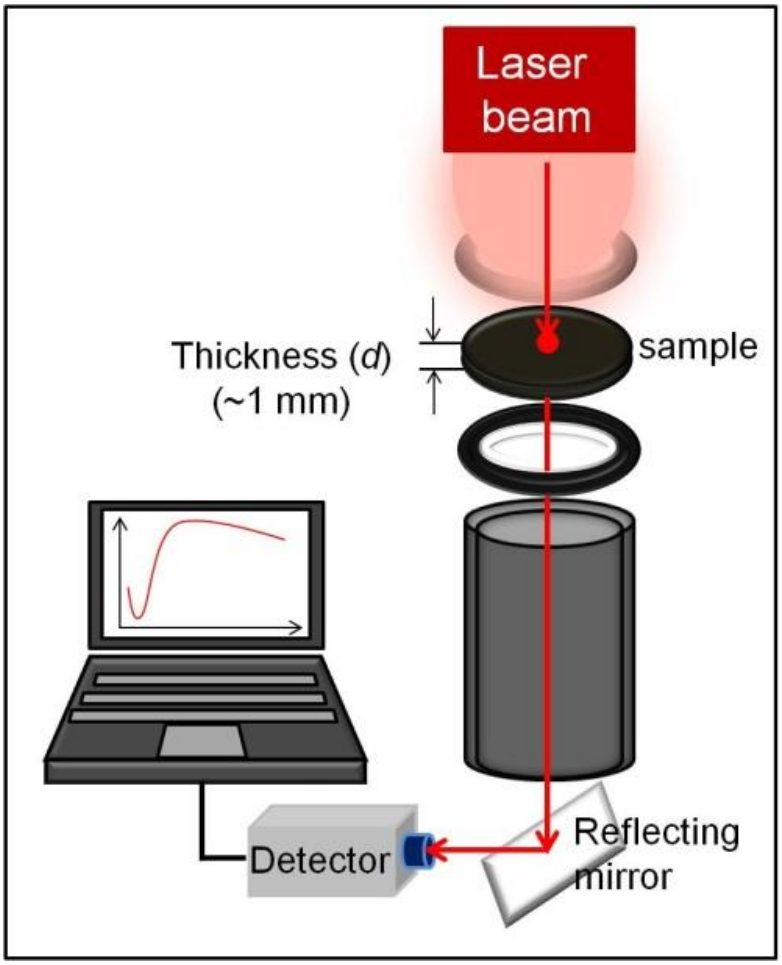

Fig. 2-3. Shematic illustration experiment setting for thermal diffusivity (a laser flash method) measurement.

2.5.2. Specific heat capacity

The measurement of C_p was carried out using differential scanning calorimeter (DSC). A piece of sample (~ 0.4 mm (thickness) x ~ 3 mm (diameter)) was sealed in a set of Al pans. A piece of sapphire (~14.3 mg) which has a well-define heat capacity was also sealed in a set of Al pans and used as a reference over the range of temperature to be observed. During the heating process, the sample and the sapphire are placed separately in a small chamber. The DSC system measures the difference amount of heat required to increase the temperature of a samples and reference as a function of temperature. Both the sample and reference are maintained at nearly the same temperature throughout the experiment.

2.6. Hall effects

The Van der Pauw method is a technique commonly used to measure the resistivity and the hall coefficient of the samples, so that several following properties can also be calculated as:

1. The doping type of the current carrier (n-type or p-type).
2. The sheet carrier density (carrier concentration/unit area).
3. The mobility of current carrier.

When a charge particle, such as an electron is placed in a magnetic field, it experiences a Lorentz force proportional to the strength of the field and the velocity at which it is travelling through it. The strongest force will occur when the direction of motion is perpendicular to the direction of the magnetic field [9].

$$F_L = qvB \tag{2-24}$$

where q is the charge on the particle (Coulomb, C), v is velocity of the particles (cm/s) and B is the strength of magnetic field (Wb/cm^2).

Then, a current is applied to a piece of semiconducting materials will result

a steady flow of electrons though the materials. Therefore, the velocity of electrons can define as:

$$v = \frac{I}{nAe} \tag{2-25}$$

where n is the electron density, A is the cross-section area of the materials and e is the electronic charge.

When an external magnetic field is applied perpendicular to the direction of current movement, the resulting Lorentz force will cause the accumulation of electrons at one surface of the sample. This accumulation will create an electric field across the material due to the uneven distribution of charge and lead to a potential difference across the material, known as Hall voltage (V_H). The magnitude of Hall voltage can be defined as:

$$V_H = \frac{IB}{end} \tag{2-26}$$

$$n = \frac{n_s}{d} \tag{2-27}$$

so:

$$V_H = \frac{IB}{en_s} \tag{2-28}$$

where n is the density of electrons, n_s is the sheet density of electrons and d is the depth of the material.

The resistivity (ρ) in the semiconductor materials can be shown to be:

$$\rho = \frac{1}{en_m\mu_m} \tag{2-29}$$

$$n_m = n_s.d \text{ and } \rho = \frac{R_s}{d} \tag{2-30}$$

where n_m, μ_m, n_s and R_s are the doping level, mobility of the majority carrier, sheet density and sheet resistance respectively. Therefore, the Hall

mobility can be express as:

$$\mu_H = \frac{1}{en_sR_s} \tag{2-31}$$

The resistance measurement is carried out without the magnetic field applied to the sample and determined using Ohm's law. As shown in Fig. 2-4, the sheet resistance can be express as:

$$R_{12,34} = \frac{V_{3,4}}{I_{1,2}} \tag{2-32}$$

Here, the sheet resistance is situated into two directions as:

$$R_{vertical} = \frac{R_{12,34}+R_{34,12}}{2} \text{ and } R_{horizontal} = \frac{R_{23,41}+R_{41,23}}{2} \tag{2-33}$$

Then the Van der Pauw formula becomes

$$e^{-\pi tR_{vertical}/\rho} + e^{-\pi tR_{horizontal}/\rho} = 1 \tag{2-34}$$

where t is the thickness of the sample.

If the samples possesses a line of symmetry where $R_{12,34} = R_{32,12}$ then ρ can be easily found as:

$$\rho = \frac{\pi t}{ln2} R_{12,34} \tag{2-35}$$

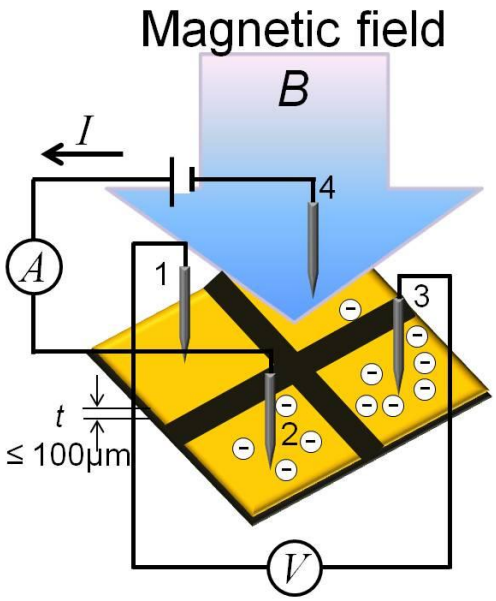

Fig 2-4. Schematic illustration of the sample for Hall effects measureme

In this experiment, Hall effect measurement was carried out using the ResiTest8300 (Toyo Tech.Co.:)at room temperature. The sample was cut and polished into the dimension of ~ 10 mm (diameter) x ~ 80 μm (thickness). The surface of the sample was then applied with an Au sputtering for better contact between the surface of the sample and the four probes. The Au sputtering areas were pointed out in the yellow color as shown in Fig 2-4.

2.7. Sound velocity

Sound velocity is a distance travelled by a sound wave during a unit of time propagating through an elastic medium. In solids, waves propagate as two types. First, a longitudinal wave (V_L) is associated with compression and de compression in the direction of travel. Second, a transverse wave (V_T) is due to elastic deformation of the medium [10]. In the misfit layer sulfide, transverse wave has 2 modes or polarizations, first

is $V_{T1;}$ the elastic deformation of the medium perpendicular to the direction of wave travel (along y and z axis), second is V_{T2}; the elastic deformation of the medium parallel to the direction of wave travel (along x and y axis). V_L is mainly influenced by Influenced by chemical bonding and the density, V_{T1} is mainly determined by interlayer bonding while V_{T2} is mainly determined by intralayer bonding [11]. The illustration as shown in Fig. 2-5.

Sound velocity measurement was carried out to examine the phonon mean free path (l) of the samples as follow:

$$\kappa_{lattice} = \frac{1}{3} c_v \,.\, l.\, \mathrm{V} \qquad (2\text{-}36)$$

where c_v is specific heat capacity (J/gK), l is phonon mean free path (nm) and V is sound velocity (m/s).

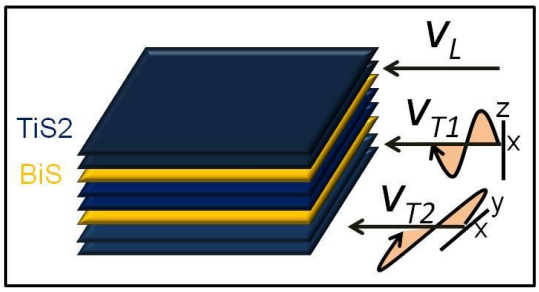

Fig 2-5. Schematic illustration of the sample for sound velocity measurement.

The sound velocity measurement is conducted by using the ultrasonic pulse–echo method (Model 5800 PR, Olympus) at room temperature. The input attent, output attent and voltage gain were set at 30 dB, 9 dB and 40 dB, respectively.

The surface of the samples was polished smoothly. For V_L measurement the surface of the samples was smeared with the couplant B

whereas the V_T with the couplant SWC. The sound velocity V is determined by the equation as follows:

$$V = \frac{2d}{\Delta t} \tag{2-37}$$

where d is the thickness of the samples (m) and Δt is the time difference between 2 peaks of the observed waves (s), as shown in Fig. 2-6.

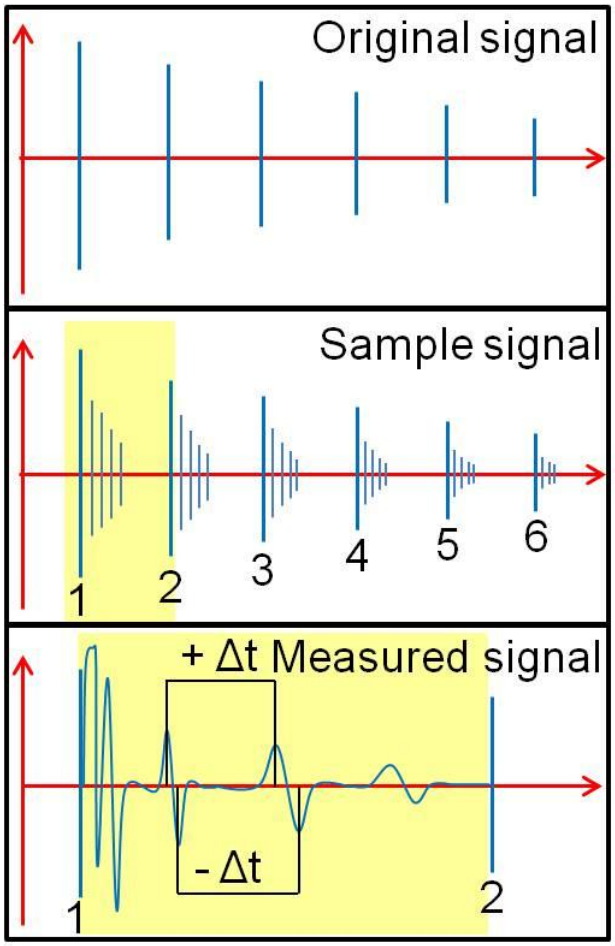

Fig 2-6. The schematic illustration of the signal in sound velocity measurement.

References

[1] G.A. Slack, New Materials and Performance Limits for Thermoelectric Cooling, in: D.M. Rowe, CRC Handbook of Thermoelectric, CRC Press: Boca Raton, FL, USA, (1995) pp.407–440.

[2] S.M. Sze, Semi Conductor Devices, 2nd ed., Wiley, USA (2001).

[3] G. Woan, The Cambridge Handbook of Physics Formulas, Cambridge University Press (2010).

[4] S. Iwanaga, E. S. Toberer, A. LaLonde, and G. Jeffrey Snyder, Review of Scientific Instruments 82 (2011) 0639051-0639056.

[5] Z. Zhou and C. Uher, Review of Scientific Instruments 76 (2005) 023901-023905.

[6] I. A. Nishida, “Measurement of Electrical Properties”, CRC Handbook of Thermoelectrics, CRC Press LLC, Boca Raton (1995) 157-164.

[7] L.I. Anatychuk, Physics of Thermoelectricity, Institute of Thermoelectricity, Ukraine (1998).

[8] J.A. Cape and G.W. Lehman, J. Appl. Phys. 34 (1963).

[9] N. A. Sinitsyn, Journal of Physics: Condensed Matter 20 (2008).

[10] Lawrence E. Kinsler, Austin R. Frey, Allan B. Coppens, James V. Sanders, Fundamentals of acoustics, 4th Ed., John Wiley and sons Inc., New York, USA (2000).

[11] Chunlei Wan, Yifeng Wang, Ning Wang and Kunihito Koumoto, Materials 3 (2010) 2606–2617.

Chapter III

Effects of Alkaline Earth Doping on The Thermoelectric Properties of $(BiS)_{1.2}(TiS_2)_2$ Misfit Layer Sulfide

3.1. Preface

The increasing worldwide energy demand has attracted a great deal of attention and consideration for the future of humankind. One of the solutions to this problem is to reduce energy waste by recycling it into usable energy. Thermoelectric materials provide an effective loophole for this problem because they can convert thermal energy into electric by utilizing the Seebeck effect [1]. Thermoelectric materials are evaluated by the dimensionless figure of merit, $ZT = S^2\sigma T/\kappa$, where S, σ, and κ are Seebeck coefficient, electrical conductivity, and thermal conductivity, respectively, at a given absolute temperature, T [2]. Higher ZT gives rise to higher thermoelectric conversion efficiency.

The $(BiS)_{1.2}(TiS_2)_2$ misfit layer sulfide has been reported as a promising thermoelectric material [2]. It was constructed by alternately stacking CdI_2 type TiS_2 trigonal, anti-prismatic layers and distorted, rock-salt type of BiS layers [3–5]. In the $(BiS)_{1.2}(TiS_2)_2$ misfit layer sulfide, titanium disulfide is a host layer where the electron transport occurs, and bismuth sulfide serves as a phonon barrier layer, which scatters the phonons and blocks the heat transport both along and across the host layers [6]. Titanium disulfide is known to possess a large power factor (S^2/ρ), but its high thermal conductivity limits its TE performance, due to a rather low ZT value at room temperature [7]. In order to increase ZT, thermal conductivity must be reduced without degrading the high power factor, for instance by intercalating bismuth sulfide (BiS) into the van der Waals gap. The intercalation of BiS layer in the van der Waals gap of TiS_2 successfully reduced thermal conductivity and even contributed to an ultralow lattice thermal conductivity at higher temperature. However, the decrease in the thermal conductivity also increases electrical conductivity too much, because electron transfer from BiS to TiS_2 layers increases the carrier concentration. Although the lattice thermal conductivity can be reduced dramatically by intercalation, increased carrier concentration

leads to larger electronic thermal conductivity and suppresses the reduction of total thermal conductivity. As a result, both the Seebeck coefficient and the power factor decrease [8].

Accordingly, we attempt in the present study to decrease the carrier concentration by doping electron acceptors in two different ways: either by substituting magnesium (Mg^{2+}) for titanium (Ti^{4+}) in the host layers, forming $(BiS)_{1.2}(Mg_xTi_{1-x}S_2)_2$, or else calcium ($Ca^{2+}$) and strontium — for bismuth ($Bi^{3+)}$ in the phonon barrier layers, forming $(Bi_{1-x}(Ca,Sr)_xS)_{1.2}(TiS_2)_2$.

3.2. Experimental procedure

The samples were prepared by a solid-state reaction method [9] and the flow chart of the experimental procedure is shown in Fig. 3-1. Elementary titanium (99.9 wt %), magnesium sulfide (99.5 wt %), bismuth (99.95 wt %), calcium sulfide (99.5 wt %), strontium sulfide (99 wt %) and sulfur (99.99 wt %) were used as starting materials. The samples with corresponding starting materials were weighted according to the stoichiometric ratio and the target composition is shown in the table 3-1. The chemical powders were put in the sealed bottle and mixed for two hours in the milling machine. The powder was mounted and then sealed in an evacuated silica tube with a length of ~15 cm outer diameter ~15 mm and inner diameter 13 mm. The powder in the sealed silica tube was fired in the furnace; the heating program as shown in Fig 3-2. The resultant powders were grinded and sieved with the sieved size of 212 μm. the Spark Plasma Sintering (SPS) was carried out to compact the powder into pellet. The powder sample (~5.5 gram) was mounted to the carbon die with the diameter size of 15 mm. The temperature and pressure program of SPS are shown in the Fig. 3-3 including with the final shape and size of the pellet. The relative density of all pellet were higher than 95 % of the theoretical values and thermoelectric measurements were carried out in the directions perpendicular to the pressure applied during sintering.

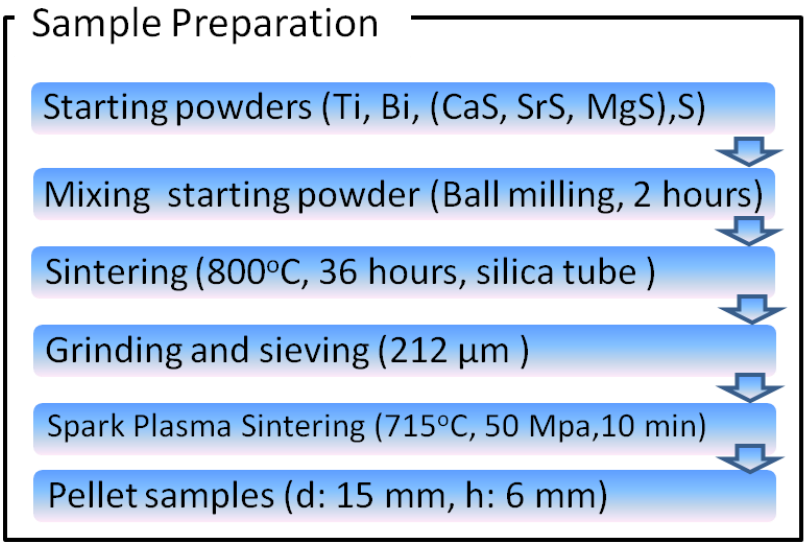

Fig.3-1. Flow chart of the experimental procedure for $(BiS)_{1.2}(TiS_2)_2$ doped samples.

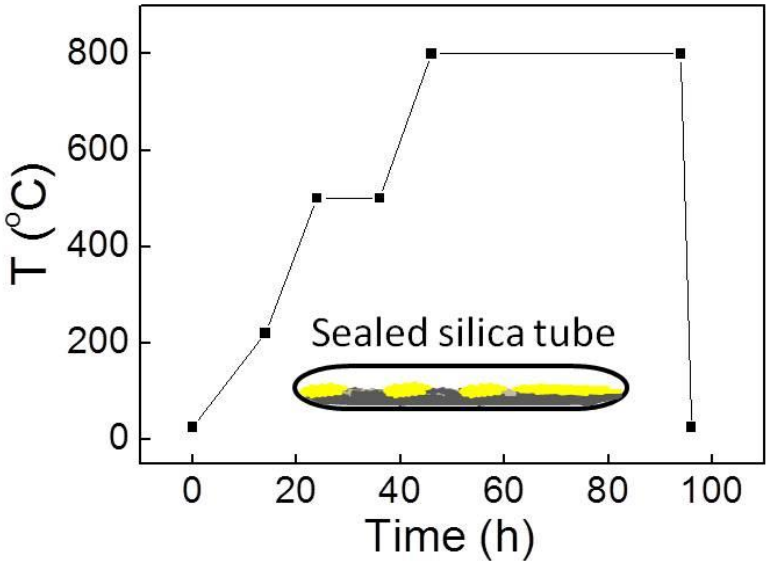

Fig. 3-2. The sintering temperature program of furnace for fabrication of the samples.

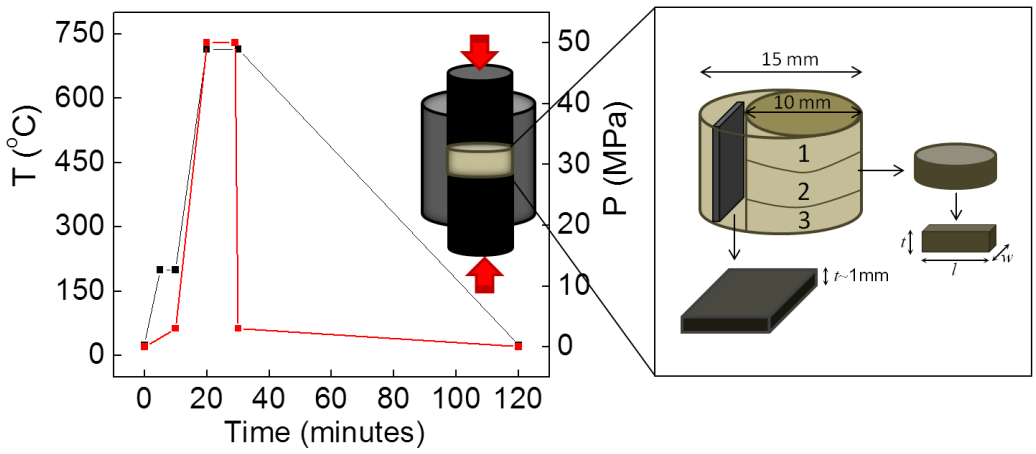

Fig. 3-3. The temperature and pressure program of spark plasma sintering (SPS) for densification of the samples.

3.3. Results and discussion

3.3.1. Morphology observation and structural analysis

The morphology observation was carried out by SEM for powder and pellet samples. Fig. 3-4 shows the powder samples have plate-like shape particles with the average size of 5-10 μm whereas the pellet samples have well align particles. The pellet shows that the samples are dense and the relative density is over 96%.

The measurement of XRD was carried out for the resultant powder and the pellet. The XRD patterns of the powder and the surface of the pellet perpendicular to the pressing direction are shown in Fig. 3-5. Several strong peaks are all related to a set of planes (0 0 *l*) perpendicular to the *c*-axis. The XRD patterns of the doped misfit layer sulfides with different doping amount matched well with that of $(BiS)_{1.2}(TiS_2)_2$, indicating that the doped misfit layer sulfide have a crystal structure similar to $(BiS)_{1.2}(TiS_2)_2$ [10]. Moreover, the substitution of Mg^{2+} into the Ti^{4+} site or Ca^{2+} and $Sr2^{+}$ into the Bi^{3+} site results in a slight shift of (006) peak due to

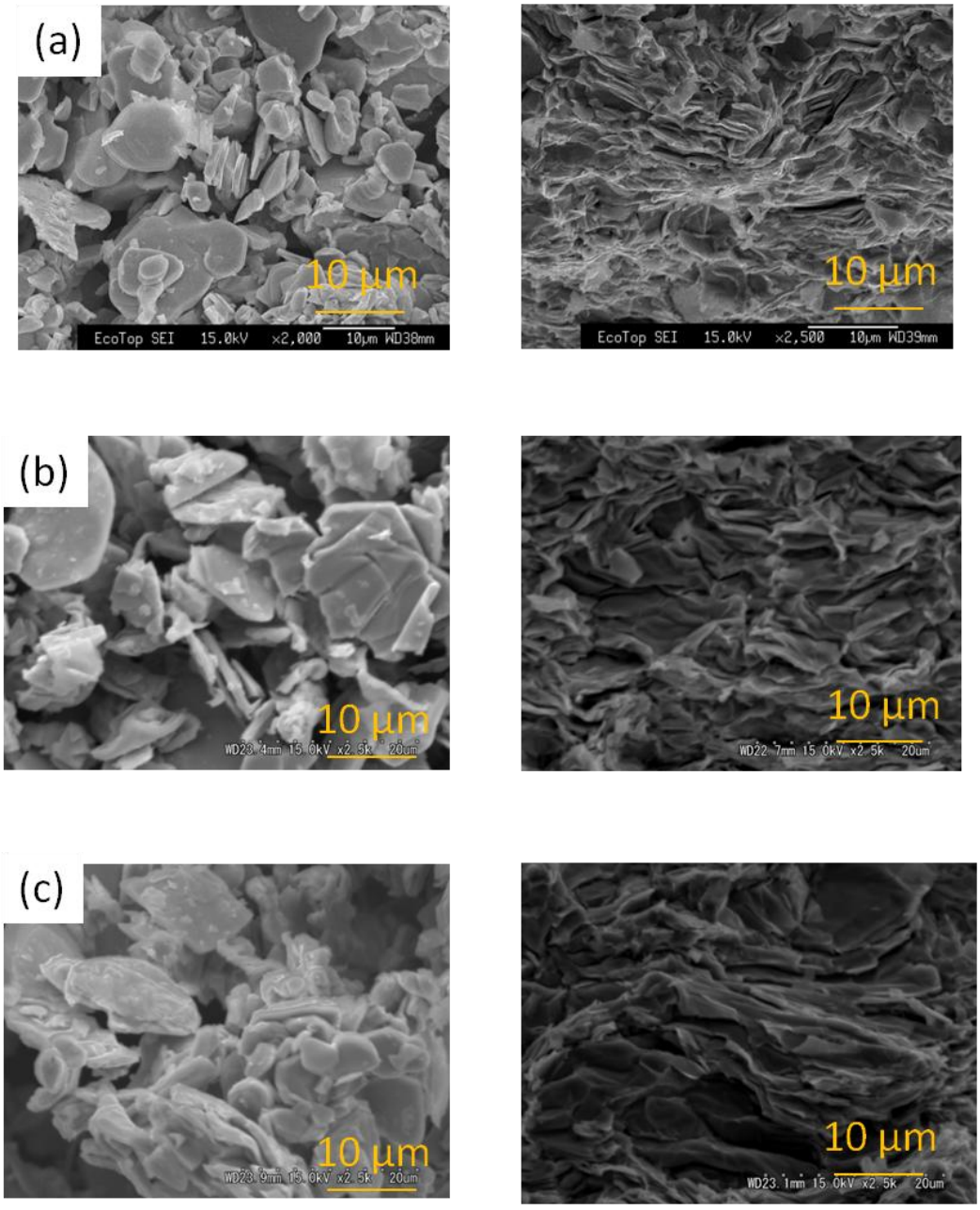

Fig. 3-4. SEM images of the powder and pellet samples
(a) $(BiS)_{1.2}(Mg_{0.05}Ti_{0.95}S_2)_2$ (b) $(Bi_{0.9}Sr_{0.1}S)_{1.2}(TiS_2)_2$
(c)$(Bi_{0.9}Ca_{0.1}S)_{1.2}(TiS_2)_2$.

the difference in the ionic radii of calcium, strontium, magnesium and the corresponding host atoms, bismuth and titanium.

All values of lattice parameter *c* were calculated from the XRD data. The calcium substitution into the bismuth site decreased the lattice parameter *c*, because the calcium ionic radius (Ca^{2+}:1.14 pm) is smaller than bismuth ionic radius (Bi^{3+}:1.17 pm). The lattice shrinks and the layers get closer to each other [11.12]. However, magnesium and strontium substitution increased the lattice parameter *c*, because the magnesium ionic radius (Mg^{2+}:72 pm) is larger than titanium ionic radius (Ti^{4+}:60.5 pm), and the strontium ionic radius (Sr^{2+}:1.32 pm) is larger than bismuth ionic radius, and as a result the layer spacing widens are shown in Fig. 3-5.

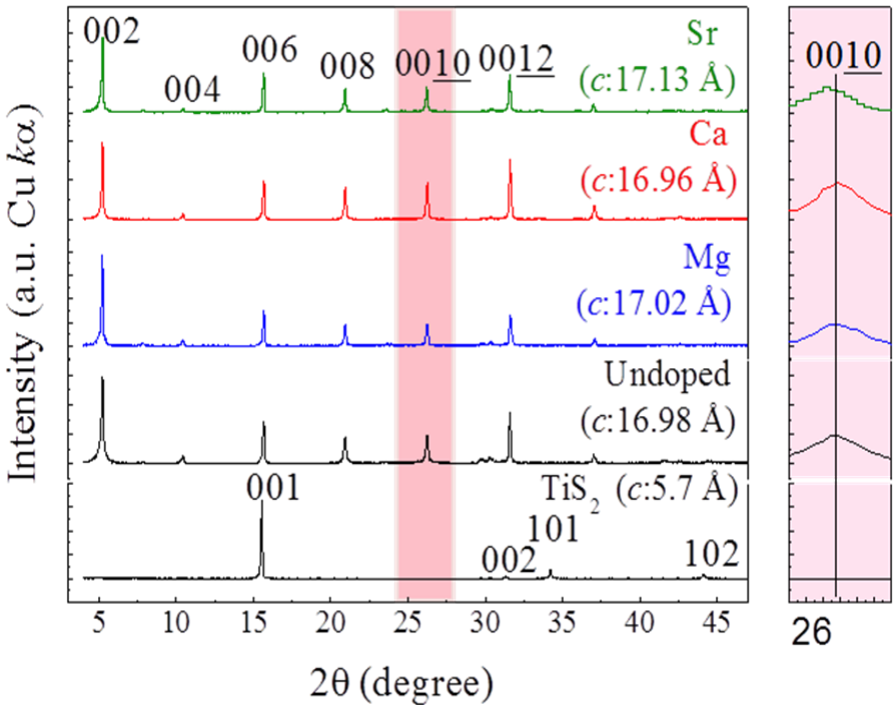

Fig. 3-5. XRD patterns of pellet samples and the lattice spacing (*c*) of each sample.

3.3.2. Thermoelectric properties

The measurement of thermoelectric parameters (σ, S, κ) were carried out at the temperature range of 300-750 K.

3.3.2.1. Electrical conductivity

The decrease in electrical conductivity with increasing temperature over the whole temperature range indicates that all compounds are metallic conductors [13]. As described previously in chapter I that TiS_2 possess semi conductor behavior if the layers are less than 10 layers but if more will be conductor. Fig. 3-6 shows that calcium, strontium, and magnesium doping all decreased electrical conductivity of $(BiS)_{1.2}(TiS_2)_2$.

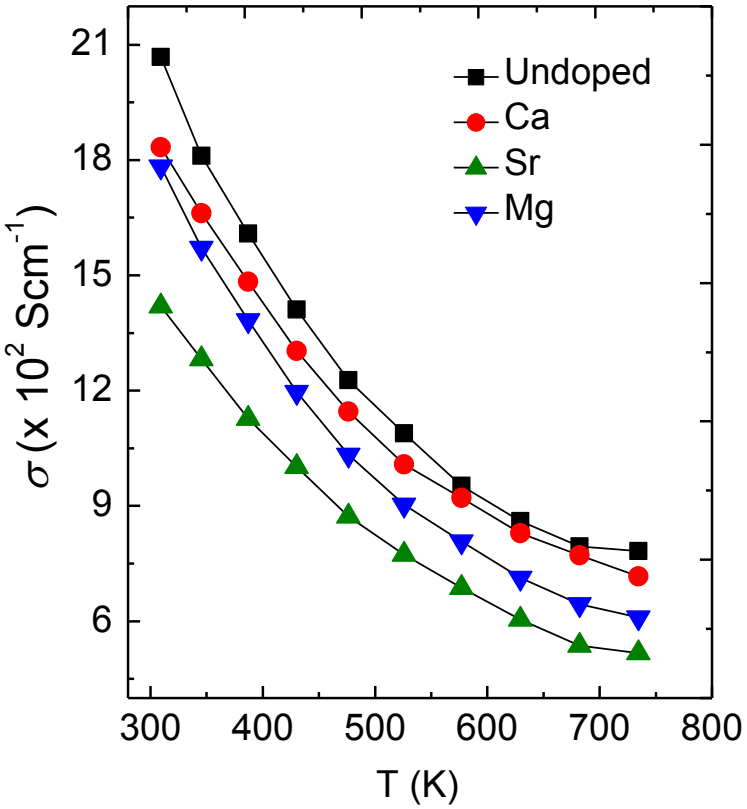

Fig.3-6. Electrical conductivity of alkaline earth doped samples.

Table 3-1. Carrier concentration, Hall mobility, and effective mass of $(BiS)_{1.2}(TiS_2)_2$, $(Bi_{0.9}Ca_{0.1}S)_{1.2}(TiS_2)_2$ $(Bi_{0.9}Sr_{0.1}S)_{1.2}(TiS_2)_2$, and $(BiS)_{1.2}(Mg_{0,05}Ti_{0.95}S_2)_2$ at room temperature.

Sample	Carrier concentration/cm^3	Hall mobility (cm^2/Vm)	Effective mass
$(BiS)_{1.2}(TiS_2)$	4.75×10^{21}	3.3	$5.7m_o$
$(Bi_{0.9}Ca_{0.1}S)_{1.2}(TiS_2)_2$	4.13×10^{21}	3.1	$4.8m_o$
$(Bi_{0.9}Sr_{0.1}S)_{1.2}(TiS_2)_2$	3.22×10^{21}	3.1	$3.5m_o$
$(BiS)_{1.2}(Mg_{0.05}Ti_{0.95}S_2)_2$	4.08×10^{21}	2.8	$4.5m_o$

Hall effects measurement was carried out to examine the type of carrier (electron or hole) and the number of carrier in the samples at room temperature. The results demonstrated that electrons were the main carriers and the number of carrier are listed in table 3-1 followed by hall mobility data. The decrease in carrier concentration due to calcium, strontium and magnesium substitution are consistent with respect to electrical conductivity. $(BiS)_{1.2}(TiS_2)_2$ misfit layer sulfide has a high carrier concentration due to the electron transfer from the phonon barrier layers, (BiS), to the host layers, (TiS_2). This electron transfer will determine the overall stability of its layer structure [14.15]. In $(BiS)_{1.2}(TiS_2)_{2,}$ 0.41 e/Ti atom fills the t_{2g} conduction band of the two TiS_2 layers, and the decrease in electron carriers due to the substitution leads to the decrease in band filling as follows: 0.35 e/Ti ($(Bi_{0.9}Ca_{0.1}S)_{1.2}(TiS_2)_2$), 0.32 e/Ti ($(Bi_{0.9}Sr_{0.1}S)_{1.2}(TiS_2)_2$), and 0.34 e/Ti ($(BiS)_{1.2}(Mg_{0.05}Ti0.95S_2)_2$). This shows that the interaction between the host layers, (TiS_2), and the phonon barrier layers, (BiS), forms the conduction electron in the TiS_2 layers and that the BiS layers may not contribute to electrical conduction [16]. The magnesium doping decreased the mobility, possibly due to the magnesium atoms disturbing the conduction paths in TiS_2 layers. In contrast, the

mobility remained unchanged in the case of calcium and strontium doping, because the BiS layer had a much smaller effect on scattering the conduction electrons [16].

3.3.2.2. Seebeck coefficient

The negative values of the Seebeck coefficient found for all the samples in the present temperature range show that the main charge carriers are electrons, in agreement with the Hall measurements. The doping of calcium and strontium for the bismuth site and magnesium for the titanium site decreased the Seebeck coefficient slightly, in spite of the decrease in carrier concentration possibly due to the decrease in carrier effective mass as shown in Fig. 3-7 and Fig. 3-8.

The density of states (DOS) effective mass of the carriers was calculated using the following equation for a metal or a degenerate semiconductor [17].

$$S = \frac{8\pi^2 k_B^2}{3eh^2} m^* T \left\{ \frac{\pi}{3n} \right\}^{2/3} \quad (3\text{-}1)$$

where n is the carrier concentration, m^* the effective mass of the carrier, k_B Boltzmann constant (1.381×10^{-23} J/K), h Plank constant (6.626×10^{-34} m^2 kg/s), e electron charge (1.602×10^{-19} C) and T is temperature (K).

The carrier mobility and the effective mass depend on the electronic structure, scattering mechanism, and structural anisotropy. In $(BiS)_{1.2}(TiS_2)_2$, the host layer (TiS_2) possesses a narrow band gap with a strong covalent bond, and behaves as a metallic conductor at all temperatures [18]. By intercalating the phonon barrier layers, (BiS), and forming $(BiS)_{1.2}(TiS_2)_2$, mobility is decreased mostly due to the increase in effective mass [19].

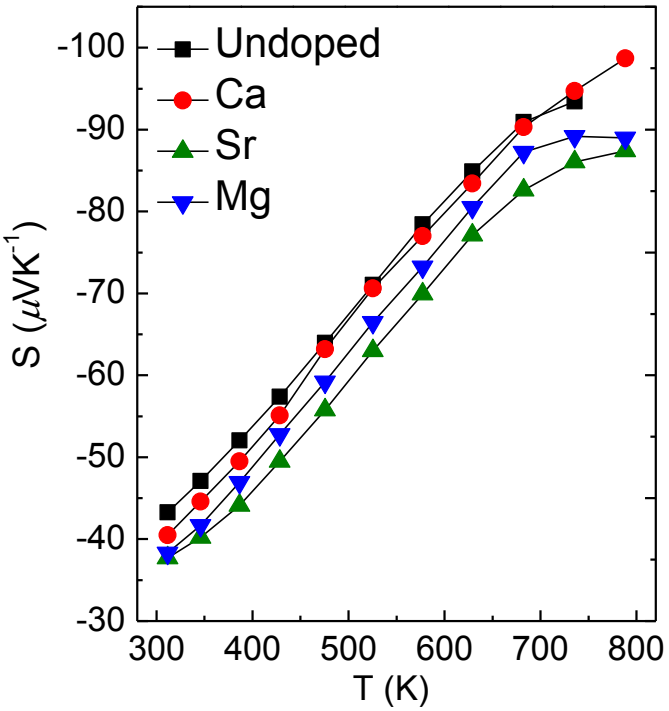

Fig.3-7. Seebeck coefficient of AE doped samples.

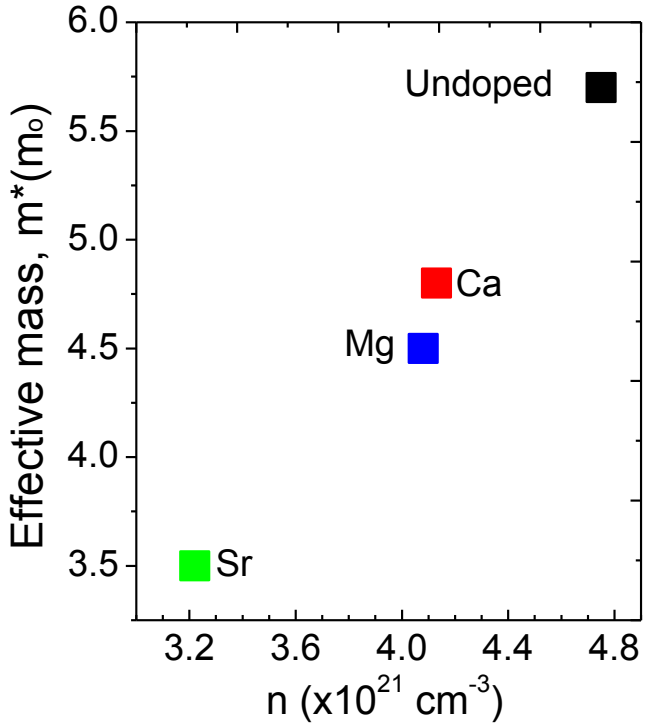

Fig. 3-8. Effective mass as a function of carrier concentration of alkaline earth doped samples.

The alkaline earth doping into different layers, magnesium into TiS_2 and calcium and strontium into BiS also has an effect on the mobility and effective mass as shown in Table 3-1. The doping decreased the effective mass, which must be due to the change in the electronic structure upon doping [16].

Since the electrical conductivity and Seebeck coefficient decreased due to the doping, the power factor also decreased overall, as shown in Fig 3-9.

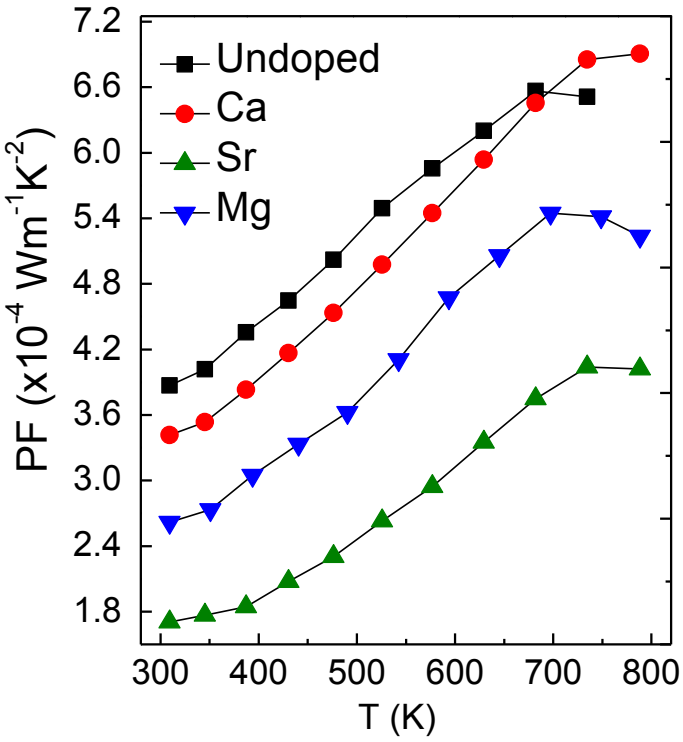

Fig. 3-9. Power factor of alkaline earth doped samples.

3.3.2.3. Thermal conductivity

The total thermal conductivity (κ) can be expressed by the sum of the electronic thermal conductivity (κ_e) and the lattice thermal conductivity (κ_l) as $\kappa = \kappa_e + \kappa_l$. We can estimate κ_e from the Wiedemann–Franz law,

$\kappa_e = \sigma \cdot L \cdot \rho$, where *L* is the Lorentz number, 2.44×10^{-8} $J^{-2}C^{-2}K^{-2}$ for free electrons [20]. Fig. 3-10(a) shows that the decrease in electrical conductivity significantly contributed to the decrease in electronic thermal conductivity (κ_e). Note that electronic thermal conductivity contributes greatly to the total thermal conductivity of $BiS(TiS_2)_2$. However, by doping either Mg^{2+} into the TiS_2 layers or Ca^{2+} into the BiS layers, we increase the thermal conductivity. On the other hands, doping Sr^{2+} into the BiS layers decrease the thermal conductivity, as shown in Fig. 3-10(a).

The phonon barrier layers, BiS, inserted into van der Waals gaps in TiS_2, enhance phonon scattering and significantly reduce the lattice thermal conductivity (κ_l). However, after doping lattice thermal conductivity also increased (Fig. 3-10(b)), although the contribution of electronic thermal conductivity decreased. We assumed that calcium and strontium doping may be responsible for the lattice matching along the *b*-axis and finally lead to the so-called “commensurate structure” [11]. In a commensurate structure, the phonon transport through the lattice has little scattering, since lattice mismatching between host layers and phonon barrier layers is eliminated as shown in simple illustration in Fig 3-11. In contrast, as shown in Fig. 3-12, magnesium substitution induced structural ordering through the elimination of planar stacking faults. The resulting ordered structure should have weaker phonon scattering compared to the disordered $BiS(TiS_2)_2$ with planar stacking faults and thus should have enhanced lattice thermal conductivity.

The substitutional doping into different layers affects lattice mismatch and hence material’s composition differently. Substitutional doping into the host layer, (TiS_2), does not change the misfit-layer structure, and the resulting composition is $(BiS)_{1.2}(Mg_{0.05}Ti_{0.95}S_2)_2$. However, substitutional doping into the phonon barrier layer, (BiS), would trigger the transition from incommensurate to commensurate structure; also, the composition would change to $(Bi_{0.9}(Ca \text{ or } Sr)_{0.1}S)_{1.2\pm x}(TiS_2)_2$ [16].

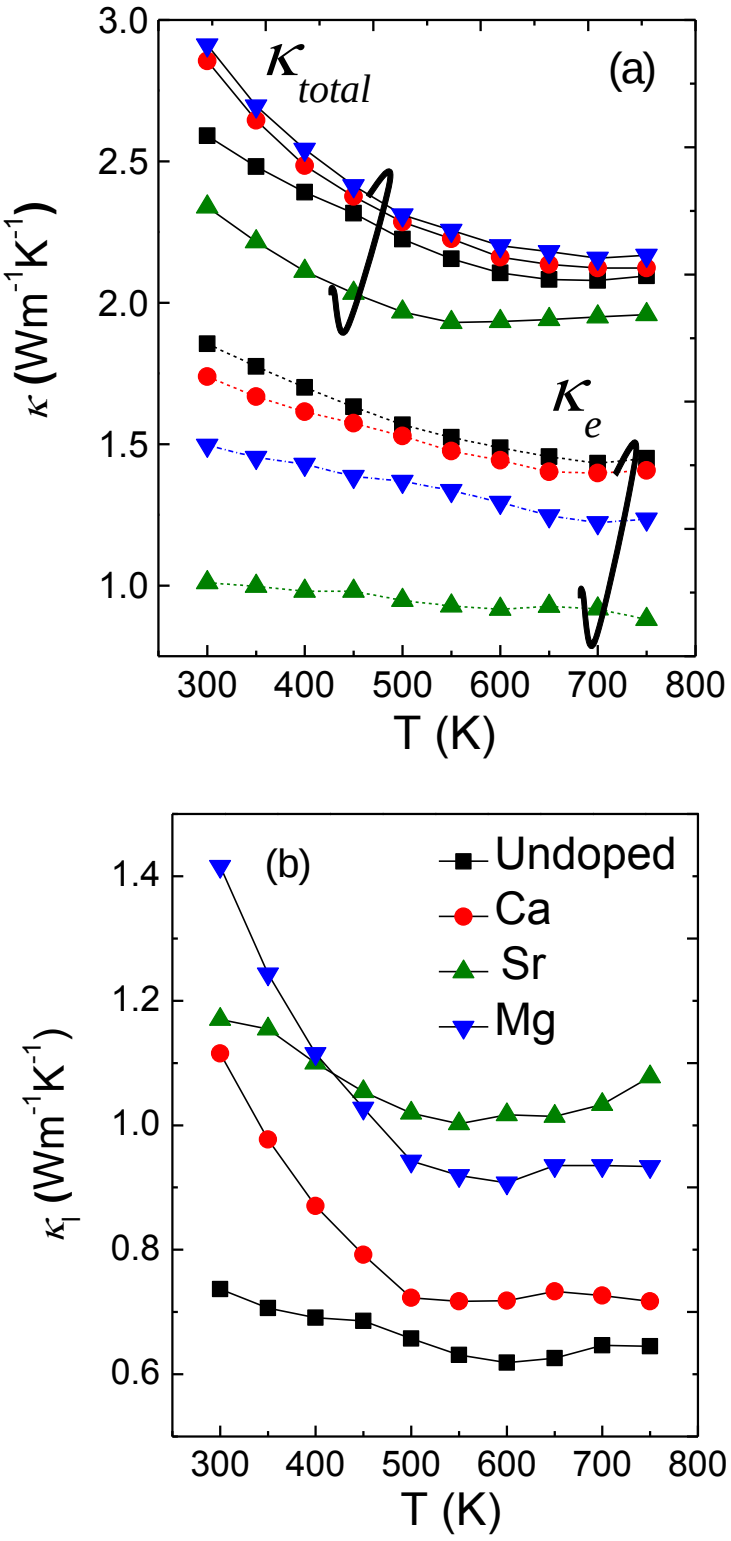

Fig.3-10. (a) Thermal conductivity and (b) Lattice thermal conductivity of alkaline earth doped samples.

The alkaline earth doping in $BiS(TiS_2)_2$ would affect the materials' stability due to the changes in interlayer bond strength, so that we measured sound velocity in the doped materials to explain the atomic bonding due to the formation of an ordered structure and a commensurate structure in the case of calcium, strontium, and magnesium doping.

The transverse polarization is a shear movement, and its velocity is closely related to the shear modulus, *G*, as expressed in the following equation:

$$V_T = \sqrt{G/\rho} \tag{3-2}$$

where *G* is the shear modulus, V_T is transverse component of sound velocity, and ρ is density [21.22].

The results are listed in table 3-2. The longitudinal sound velocity, V_L, had various values for each doping, attributed to the different values of density. The increase of density decreased longitudinal sound velocity. The transverse sound velocity 1, V_{T1}, and shear modulus 1, G_1, increased, which we speculate was due to calcium, strontium, and magnesium doping into either BiS or TiS_2 layers strengthening the covalent bonding between those dopant atoms and the sulfur atoms within the TiS_2 layers. In contrast, the magnesium substitution at the Ti site had little effect on V_{T2} and G_2, possibly because the layer-to-layer mismatch did not change. When the calcium and strontium were substituted for bismuth, leading to a commensurate structure, the intralayer bonding was reinforced, which resulted in an increase in V_{T2} and G_2. These results showed that doping into the phonon barrier layer contributed to the formation of a commensurate structure, distorting the rock salt structure.

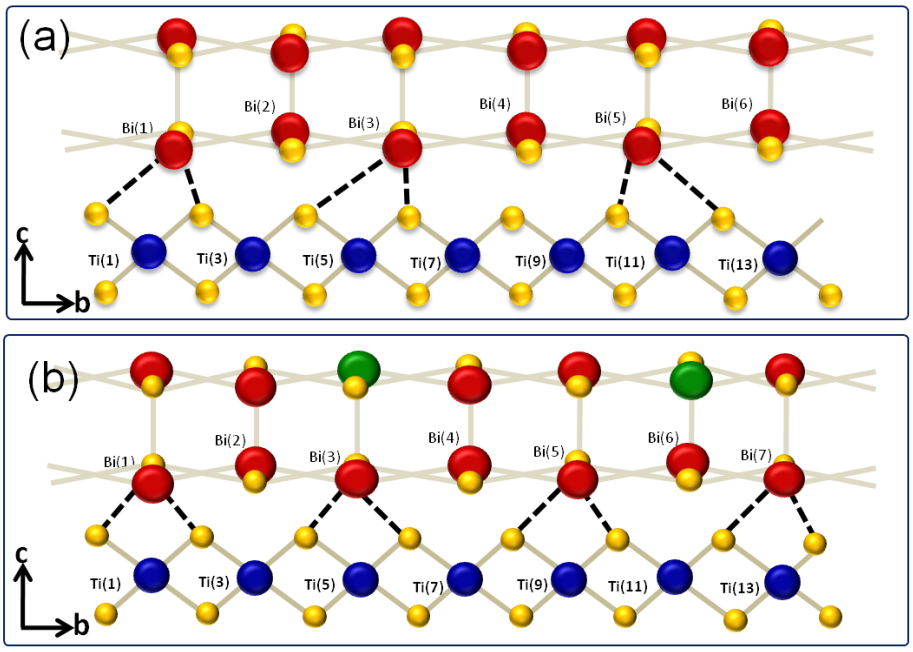

Fig. 3-11. The schematic figure of (a) incommensurate structure and (b) commensurate structure.

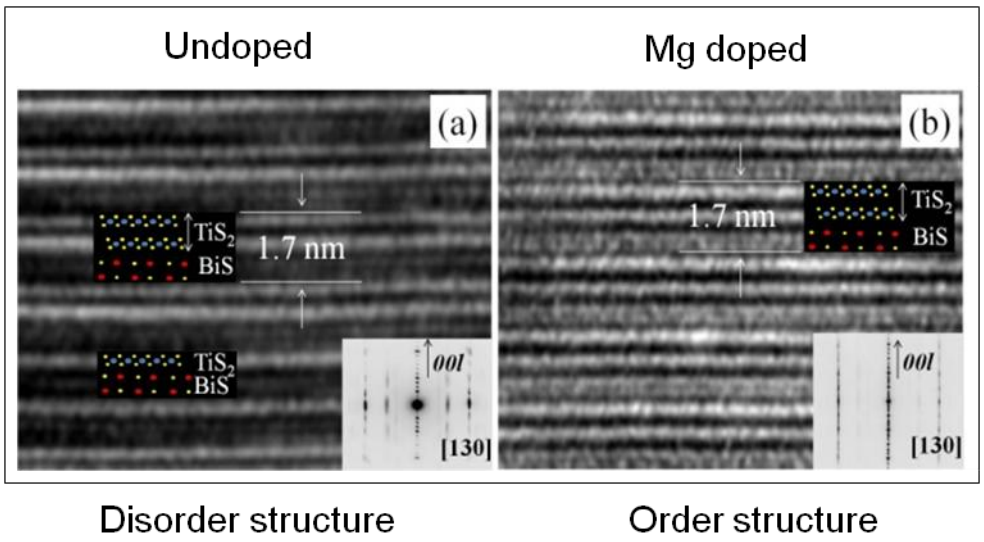

Fig. 3-12. TEM images of (a) undoped sample and (b) magnesium doped sample.

Table 3-2. Density, V_L, V_{T1}, V_{T2}, G_1, and G_2 of $(BiS)_{1.2}(TiS_2)_2$, $(Bi_{0.9}Ca_{0.1}S)_{1.2}(TiS_2)_2$, $(Bi_{0.9}Ca_{0.1}S)(TiS_2)_2$, and $(BiS)_{1.2}(Mg_{0.05}Ti_{0.95}S_2)_2$.

Sample	ρ (g/cm^3)	V_L (m/s)	V_{T1} (m/s)	V_{T2} (m/s)	G_1 (GPa)	G_2 (GPa)
$(BiS)_{1.2}(TiS_2)_2$	4.38	3596	1396	1660	8.5	12.1
$(Bi_{0.9}Ca_{0.1}S)_{1.2}(TiS_2)_2$	4.25	3862	1431	1860	8.7	14.7
$(Bi_{0.9}Sr_{0.1}S)_{1.2}(TiS_2)_2$	4.33	3439	1700	2020	12.5	17.7
$(BiS)_{1.2}(Mg_{0.05}Ti_{0.95}S_2)_2$	4.35	3596	1429	1720	8.9	12.9

3.3.2.4. Dimensionless figure of merit (*ZT*)

The *ZT* values were calculated from electrical conductivity, Seebeck coefficient, and thermal conductivity are shown in Fig. 3-13. The substitution of alkaline earth into the $BiS(TiS_2)_2$ misfit layer sulfides decreased *ZT* slightly due to the decreases in electrical conductivity, Seebeck coefficient, and the increase in thermal conductivity.

In the misfit layer sulfides, doping did decrease the carrier concentration significantly. However, the decrease in carrier concentration did not increase the Seebeck coefficient because doping distorted the electronic structure of the host layer where conduction occurred. Moreover, the formation of commensurate and ordered structure increased the lattice thermal conductivity. This phenomenon indicated that doping in the misfit layer sulfides should not disturb the electronic structure of the host layers. Therefore, the host atom and the dopant likely had close ionic radii. Nevertheless, low lattice thermal conductivity was maintained. It is likely that controlling this parameter can enhance the thermoelectric properties of this material.

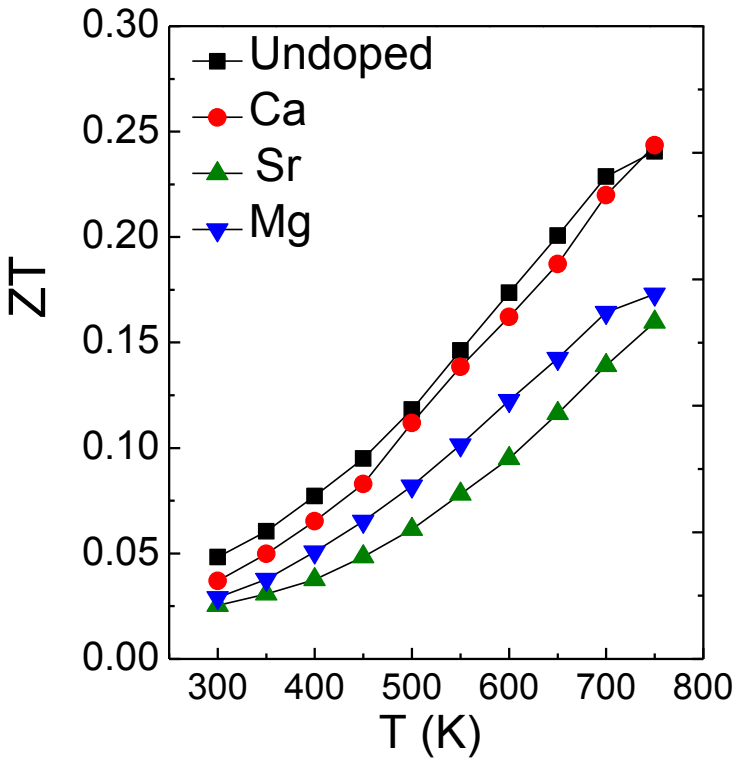

Fig. 3-13. Dimensionless figure of merit (*ZT*) value of alkaline earth doped sample.

3.3.2.5. Summary

We have investigate the influence of alkaline earth element substitution on the electrical and thermal properties of $(BiS)_{1.2}(TiS_2)_2$ misfit layer sulfides forming $(BiS)_{1.2}(Mg_xTi_{1-x}S_2)_2$ and $(Bi_{1-x}(Ca,Sr)_xS)_{1.2}(TiS_2)_2$. In the present study, we attempted to decrease the carrier concentration by doping electron acceptors. The powder samples were fabricated by solid state reaction method and compacted by spark plasma sintering (SPS) technique. XRD patterns show there are no impurity peaks and secondary phases observed in the samples. The substitution did reduce the carrier concentration and in agreement with the decrease in electrical conductivity. However, Seebeck coefficient decreased slightly due to the decrease in effective mass of carrier electrons. We have confirmed that the

incommensurate structure is essential to maintaining the low thermal conductivity of the misfit layer sulfides, as the formation of a commensurate structure by finely tuning the lattice parameter of the BiS layer increases thermal conductivity. Although the *ZT* value slightly decreased due to alkaline earth element substitution, efforts should still be made to improve the thermoelectric performance of these misfit layer sulfides.

References

[1] G. D. Mahan and J. 0. Sofo , Appl.Phys. Sci. 93 (1996) 7436-7439.

[2] Chunlei Wan, Yifeng Wang, Ning Wang and Kunihito Koumoto, Materials 3 (2010) 2606–2617.

[3] E. Guilmeau, Y. Breard, A. Maignan, Applied Physics Letters 99 (2011) 052107.

[4] M.S. Whittingham, Prog. Solid State Chem. 12 (1978) 41.

[5] G.A. Wiegers, Prog. Solid St. Chem. 24 (1996)1–139.

[6] G.A. Wiegers, J. Alloys Compd 219 (1995)152–156.

[7] H. Imai, Y. Shimakawa,Y. Kubo, *Phys. Rev.* B 64 (2001) 241104 (R).

[8] C.L. Wan, Y.F. Wang, N. Wang, Y.E. Putri, W. Norimatsu, M. Kusunoki, K. Koumoto, Layered Structure Metal Sulfides as Novel thermoelectric materials, in: D.M. Rowe, Modules, System and Application in Thermoelectric, CRC Press: Boca Raton, FL, USA, 2012:4.1–4.11.

[9] Y. Oosawa, Y. Gotoh, M. Onoda, Chem. Lett. 52. 3 (1989).

[10] A.L. Let et al., J. Phys. Chem. Solids 68(2007) 1428–1435.

[11] Yi-Chug Hung, Shiou-Jyh Hwu ,Inorg. Chem. 32 (1993) 5427–5428.

[12] X.Y. Qin et al, J. Appl. Phys.102 (2007) 073703.

[13] J. Zhang, X.Y.Qin, H.X. Xin, D.Li, C.J.Song, J. Electron. Mater. 4 (2011)

[14] J. Rouxel, A. Meerschaut, G.A. Wiegers, J. Alloys Compd. 229 (1995) 144–157.

[15] Sergey P. Abramov, J. Alloys Compd 259 (1997) 212–218.

[16] Chunlei Wan et al, J. Electron Mater 49. 5 (2011) 1271–1280.

[17] G.J. Snyder, and E.S. Toberer, Nat. Mater. 7 (2008) 105–114.

[18] Z.Y. Wu et al, Phys. Rev. B 54. 16 (1996).

[19] Lawrence E. Condry and Kyu Chang Park, Inorg. Chem 7. 3 (1968) 459–463.

[20] J. Zhang, X.Y. Qin, D. Li, H.X. Xin, L. Pan, K.X. Zhang, J. Alloy Compd. 479. 816 (2009).

[21] C.M.Fang, R.A de Groot, G A Wiegers and C Haas, J. Phys.: Condens. Matter 8 (1996) 1663–1676.

[22] Y Ohno, Phys. Rev. B 44 (1991) 1281–1291.

Chapter IV

Effects of Transition Metal substitution on the Thermoelectric Properties of Metallic $(BiS)_{1.2}(TiS_2)_2$ Misfit Layer Sulfide

4.1. Preface

Thermoelectric materials can help the worldwide demand for energy by converting waste heat into electricity [1-4]. Imai *et al*. reported that a single crystal of titanium disulfide (TiS_2) is a potential thermoelectric material because of its high power factor, which is comparable with that of Bi_2Te_3 alloy at room temperature [5-8]. However, despite its large power factor, the thermoelectric performance of TiS_2 is limited by its relatively large thermal conductivity, so its *ZT* is not optimum. Reducing the thermal conductivity of TiS_2 by intercalating a bismuth sulfide (BiS) layer into the van der Waals gap to form $(BiS)_{1.2}(TiS_2)_2$ successfully reduced its lattice thermal conductivity without reducing its high power factor [9]. However, electron transfer occurs from the BiS layers to the TiS_2 layers in $(BiS)_{1.2}(TiS_2)_2$, which greatly increases its carrier concentration and electrical conductivity. As a result, the Seebeck coefficient of $(BiS)_{1.2}(TiS_2)_2$ decreases and its power factor is sub-optimum [9-11]. In our previous work, we substituted the titanium sites in TiS_2 layers and bismuth sites in BiS layers with several electron-acceptor alkaline earth (AE) dopants [11]. However, the resulting decrease in carrier concentration also led to a decrease in the Seebeck coefficient because of the lower effective mass of the AE materials. Although TiS_2 is a semiconductor with a narrow band gap, $(BiS)_{1.2}(TiS_2)_2$ can become a semi-metal because of overlap of the broad band of the BiS sublayer with that of the TiS_2 sublayer. Thus, in this work, we investigated the effect of substitution of $(BiS)_{1.2}(TiS_2)_2$ with a series transition metal (TM) elements on the thermoelectric properties of the resulting materials. Our purpose was to increase the Seebeck coefficient of the doped materials by formation of additional energy states, namely resonances around the Fermi level, to optimize thermoelectric performance.

4.2. Experimental procedure

$(BiS)_{1.2}(Ti_{0.95}TM_{0.05}S_2)_2$ samples were synthesized by a conventional solid-state technique. High-purity starting materials (Ti, Bi, S, V, Cr_2S_3, MnS, FeS, CoS, NiS, CuS, and ZnS) were combined in stoichiometric amounts and then mixed for 2 h; the preparation procedure and measurement devices have been reported elsewhere [11]. All of the pellets obtained from spark plasma sintering (SPS) had a relatively high density of over 96%. Thermoelectric properties were measured along the direction perpendicular to the pressure applied during the sintering process. The ionic states of TM dopants were analyzed by x-ray photoelectron spectroscopy (XPS; JEOL, Tokyo, Japan) using an Al Kα x-ray source.

4.3. Results and discussion

4.3.1. Structural analysis

The single phase of each synthesized bulk sample was confirmed by x-ray diffraction (XRD). XRD patterns were measured in the direction perpendicular to the applied pressure during the sintering process and are shown in Figure 4-1. The strong peaks of the (00*l*) planes show that all the samples have a strong preference to orient with the *c* axis parallel to the direction of pressure. The XRD patterns confirmed there were no substantial changes or impurity phases present in the samples other than the hexagonal phase of TiS_2, CdI_2 structure, and the cubic phase of BiS distorted rock salt structure [9.12].

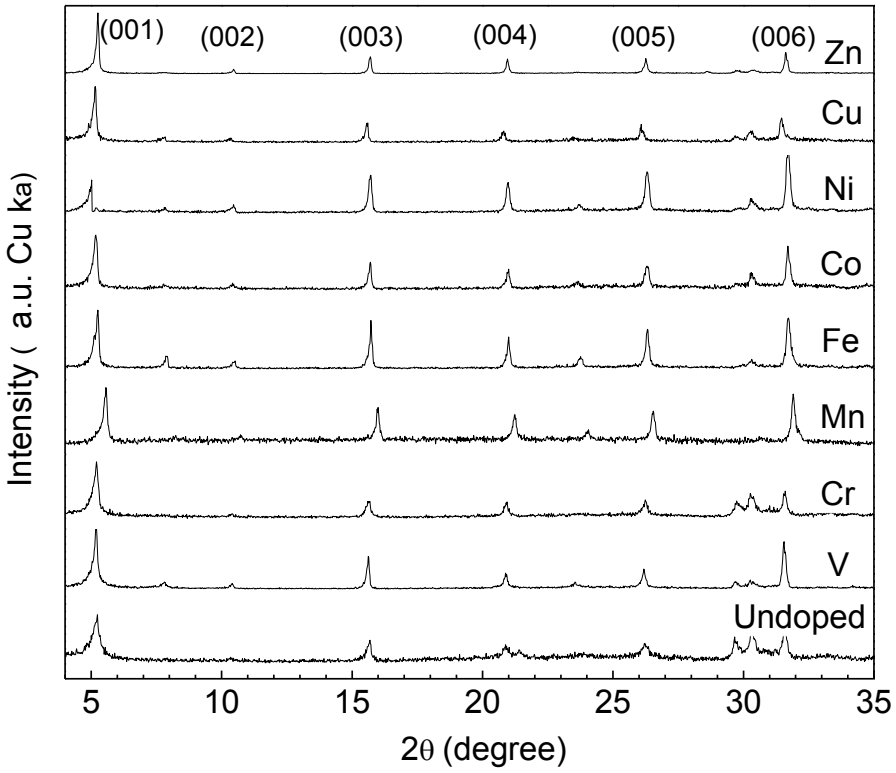

Figure 4-1. XRD pattern of TM doped samples.

4.3.2. Ionic state analysis

We performed XPS measurements to identify the ionic state of the TM dopants in the samples, the results are presented in Figure 4-2. To identify the ionic state of each TM dopant, we compared the spectra with those reported for each metal sulfide [13-20]. The spectra indicated that Cr is trivalent but V, Mn, Fe, Co, Ni, Zn, and Cu are divalent. This indicates that all of the TM ions have successfully substituted Ti^{4+} in the TiS_2 layers and behave as acceptors.

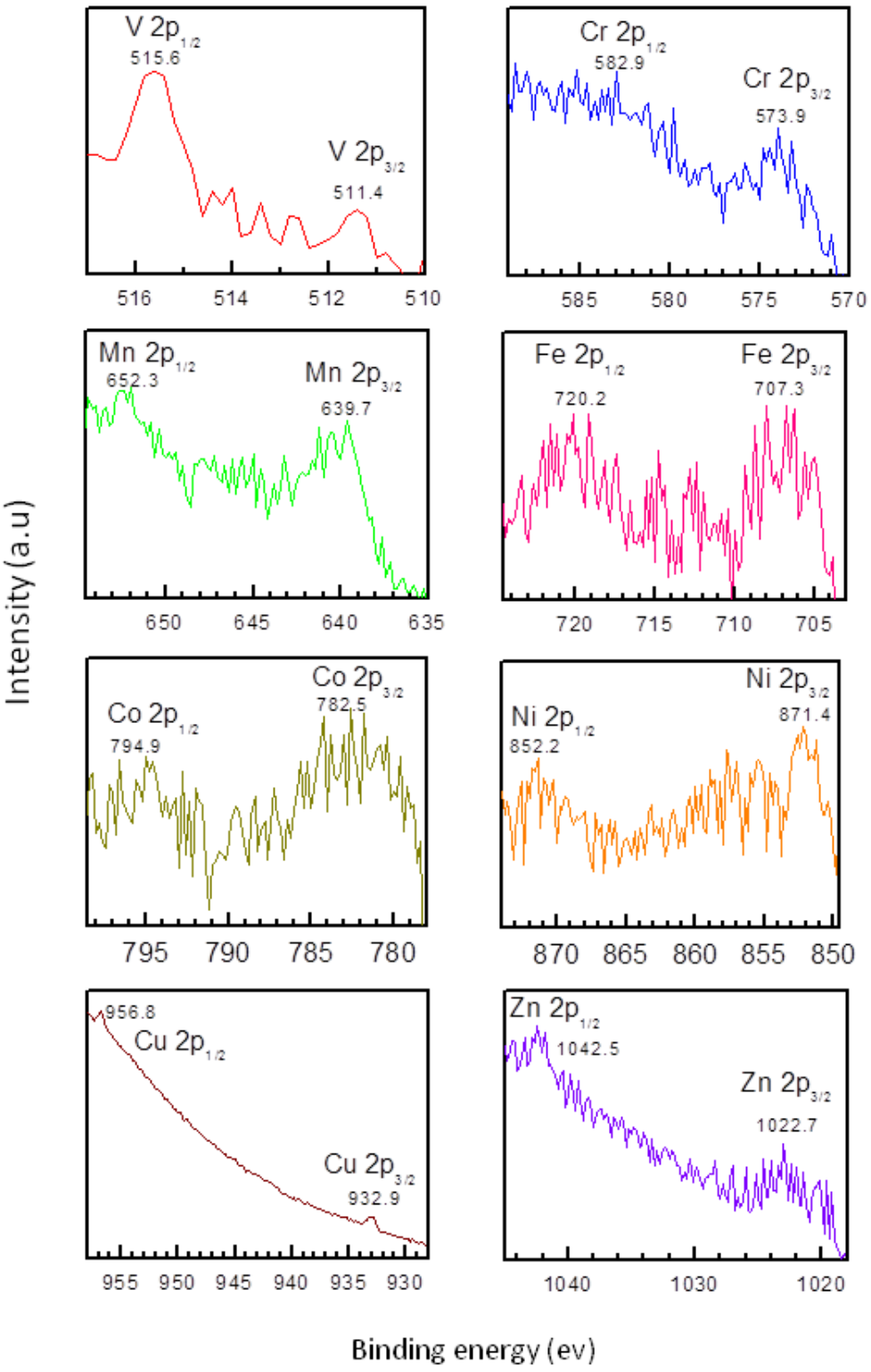

Figure 4-2. XPS spectra of TM-doped samples.

4.3.3. Thermoelectric properties

4.3.3.1. Electrical conductivity

Figure 4-3(a) shows that the substitution of titanium sites in the TiS_2 layers with TM elements substantially reduces the electrical conductivity of the resulting materials in the whole temperature range investigated. Furthermore, the temperature dependence of electrical conductivity of all samples decreases with temperature, which is indicative of metallic conduction [21]. Unlike the other doped samples, transition of electron transport behavior from metallic to semiconductor at 500 K was observed for the Fe-doped sample, indicating that the carriers in TiS_2 may be partially localized in this sample [22].

Hall measurements were conducted to examine the change in the number of carriers in the samples after doping. Table 1 shows that the TM-doped samples have fewer carriers than the undoped sample. These results indicate that the acceptor dopants have been successfully incorporated into the Ti sites (Ti^{4+}) in the TiS_2 layers, supporting the XPS results. Carrier mobility often decreases upon element substitution or doping because of the alloy scattering effect. Therefore, the large decrease in electrical conductivity of the Fe-doped sample occurred not only because of reduced carrier concentration but also because of the substantial decrease in carrier mobility, which is possibly because Fe doping alters the crystal structure [23].

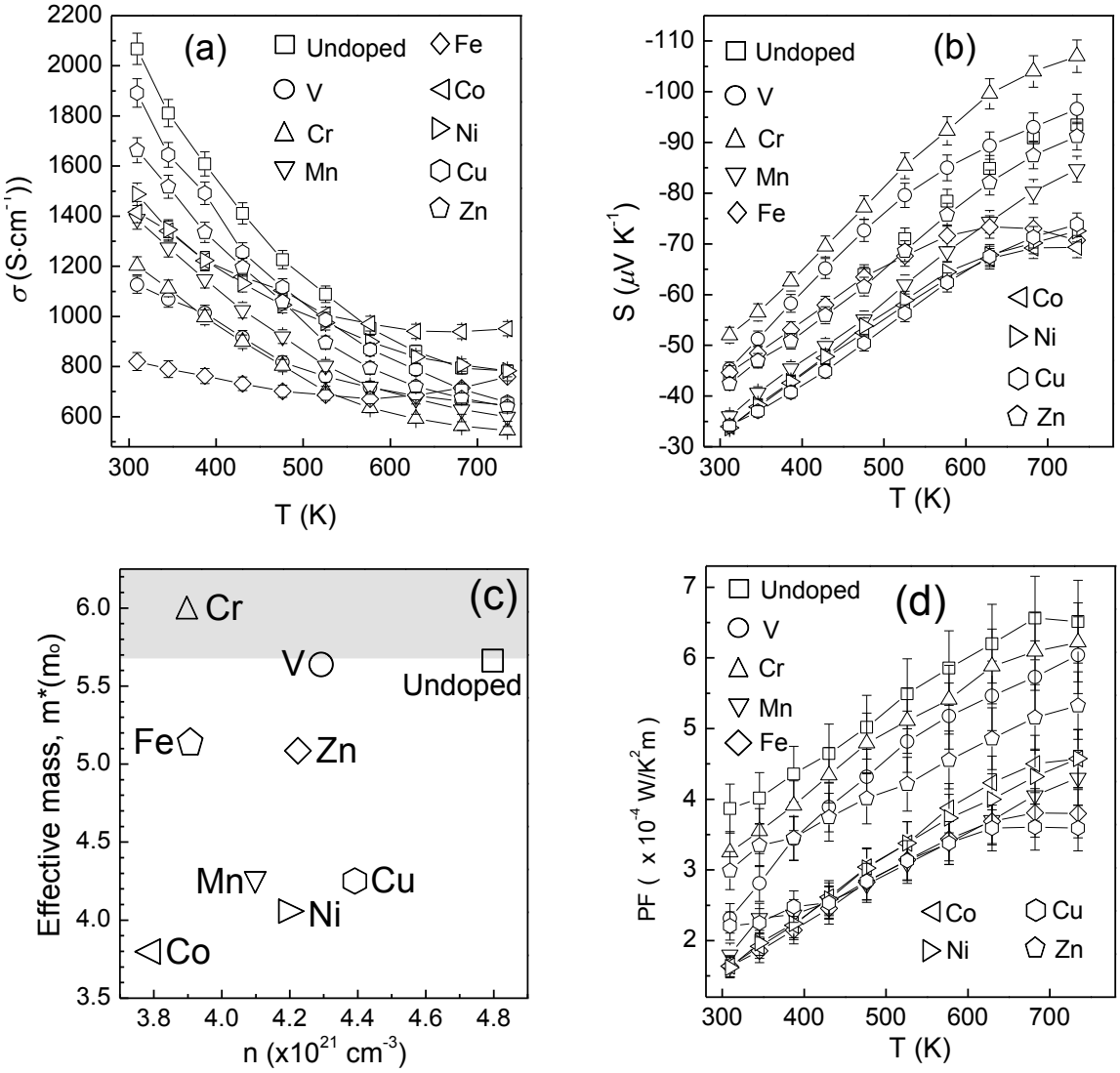

Figure 4-3. The electrical properties of TM doped samples: (a) electrical conductivity, (b) Seebeck coefficients, (c) effective mass as a function of carrier concentration, and (d) power factor.

Table 1.

Sample	Carrier concentration, n (cm^{-3})	Mobility, μ ($mv^{-1}s^{-1}$)
Undoped	4.8×10^{21}	2.8
V	4.3×10^{21}	1.9
Cr	3.9×10^{21}	2.1
Mn	4.1×10^{21}	2.2
Fe	3.9×10^{21}	1.3
Co	3.8×10^{21}	2.3
Ni	4.2×10^{21}	2.2
Cu	4.4×10^{21}	2.6
Zn	4.2×10^{21}	2.5

4.3.3.2. Seebeck coefficient

The negative Seebeck coefficients of the samples suggest that electrons are the main carriers, as shown in Figure 4-3(b). However, even though all of the TM dopants have reduced the carrier concentration, only V and Cr doping cause a large increase in the Seebeck coefficient. This increase in the Seebeck coefficient is mainly caused by the increase in the effective

mass of the carriers in these samples, as shown in Figure 4-3(c), which depicts the effective mass of the carriers as a function of carrier concentration. Effective mass was calculated by use of the following expression for the Seebeck coefficient of a metal or degenerate semiconductor, assuming a single parabolic band and energy-independent carrier scattering [2]:

$$S = \frac{8\pi^2 k_B^2}{3eh^2} m^* T \left\{ \frac{\pi}{3n} \right\}^{2/3}$$

where n is the carrier concentration, m^* is the effective mass of a carrier, k_B is the Boltzmann constant (1.381×10^{-23} JK^{-1}), h is the Planck constant (6.626×10^{-34} m^2kgs^{-1}), e is the electron charge (1.602×10^{-19} C), and T is the absolute temperature (K).

TiS_2 is a narrow-band-gap semiconductor, but $(BiS)_{1.2}(TiS_2)_2$ can possibly become a semi-metal because of overlap of the bands of the BiS and TiS_2 sublayers. After TM doping, substitution of Ti with elements with *3d* orbitals possibly induces a resonance level near the Fermi level that could enhance the Seebeck coefficient [24,25]. In V and Cr-doped $(BiS)_{1.2}(TiS_2)_2$, this resonance may occur, assuming that Ti as a host atom has slightly different energy levels than those of V and Cr as dopants. Dopants with half-filled $3d_{t2g}$ orbitals result in nearly equal energy levels, thus causing a resonance and creating additional energy levels around the Fermi level. However, further investigation, for example calculation of the density of states of these compounds, is needed to prove this assumption. Figure 4-3(d) reveals that the power factor of these samples cannot be optimized because the large decrease in electrical conductivity is not outweighed by a substantial increase in the Seebeck coefficient.

4.3.3.3. Thermal conductivity

The total thermal conductivity (κ) of the TM-doped samples decreases over the whole temperature range investigated, as shown in Figure 4(a). κ is expressed as the sum of the electronic thermal conductivity (κ_e) and the lattice thermal conductivity (κ_l), *i.e.*, $\kappa = \kappa_e + \kappa_l$. As shown in Figure 4(b), the observed large decrease in thermal conductivity could be attributed mainly to the reduction of electronic thermal conductivity, which

can be approximately estimated by use of the Wiedemann-Franz law [26]. Obviously, κ could be further suppressed by maintaining low lattice thermal conductivity. Unfortunately, all of the doped samples have higher lattice thermal conductivity than pure $(BiS)_{1.2}(TiS_2)_2$, as shown in Figure 4(c).

The high-resolution transmission electron microscopy (HRTEM) images of the samples shown in Figure 4-5 reveal that the increase in the lattice thermal conductivity is caused by the new structural ordering. This new ordering occurs as a result of elimination of planar stacking faults present in the undoped sample. An HRTEM image of pristine $(BiS)_{1.2}(TiS_2)_2$ along the *a*-axis reveals different stages inside one crystal. As can be seen in Figure 4-5(a), in some parts, pairs of TiS_2 layers and a single BiS layer are stacked periodically to form the composition $(BiS)_{1.2}(TiS_2)_2$. However, in other areas, a single TiS_2 layer and one BiS layer stack alternately to form $(BiS)_{1.2}TiS_2$. The selected area electron diffraction (SAED) pattern of this image reveals diffuse reflections, confirming the substantial disorder in the stacking sequence. In contrast, Figure 4-5(b) reveals the existence of a regular assembly of two TiS_2 layers and one BiS layer, a so-called commensurate structure. The very sharp reflections in the SAED pattern of this image are also indicative of

formation of an ordered structure. The resulting ordered structure should have weaker phonon scattering than that of disordered $(BiS)_{1.2}(TiS_2)_2$ with planar stacking faults, and thus should have enhanced lattice thermal conductivity [27].

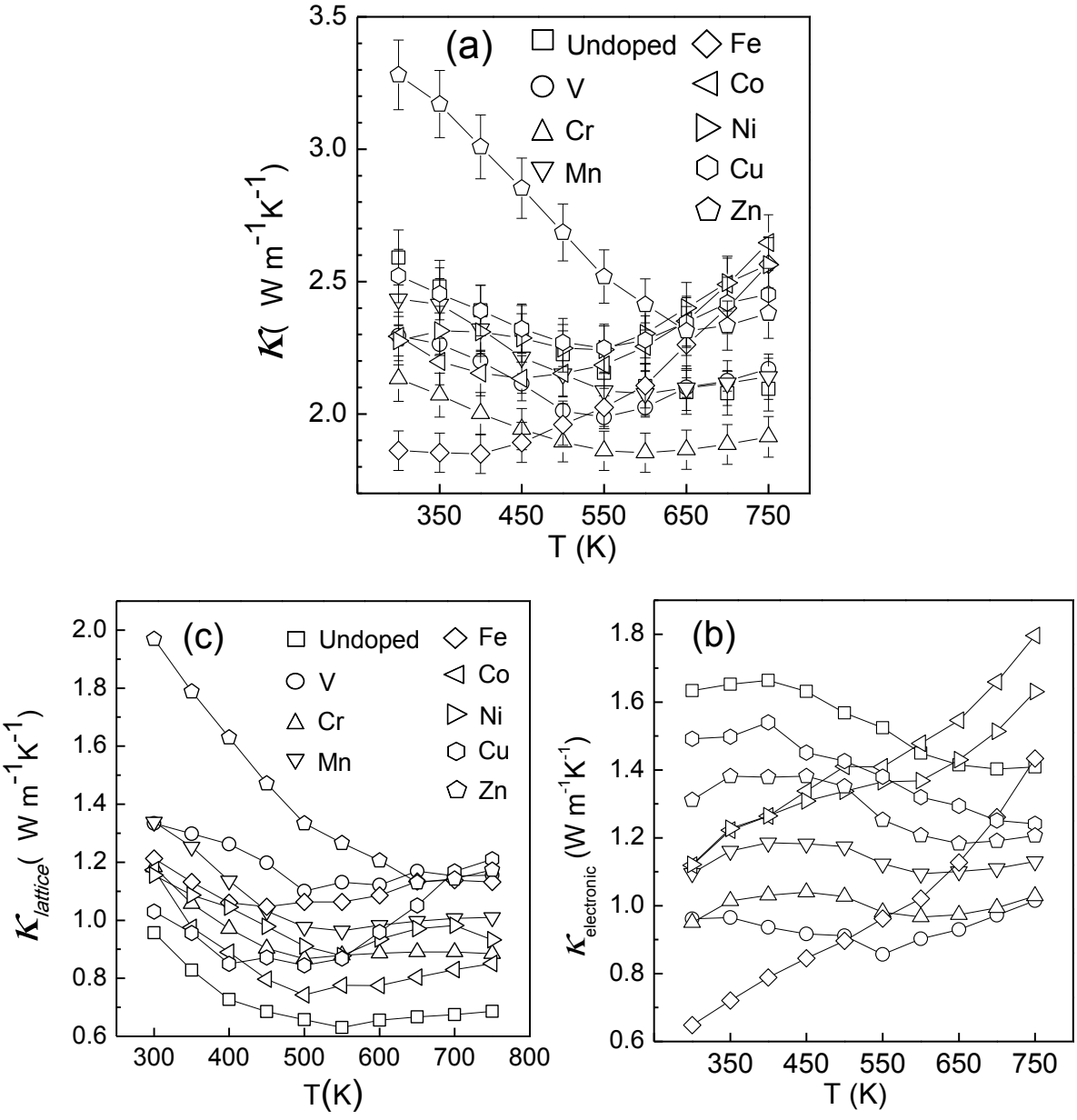

Figure 4-4. (a) thermal conductivity, (b) electronic thermal conductivity, and (c) lattice thermal conductivity of TM-doped samples.

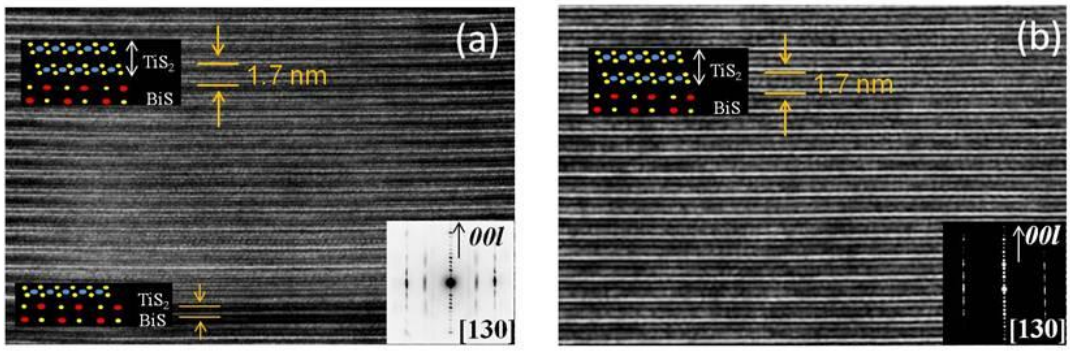

Figure 4-5. HRTEM images (a) Undoped sample and (b) chromium doped sample.

4.3.3.4. Dimensionless figure of merit (*ZT*)

Figure 4-6 shows that the Cr-doped sample has higher *ZT* than the other TM-doped samples. Although both the electrical conductivity and thermal conductivity are reduced by TM substitution, the large increase in the Seebeck coefficient of the Cr-doped sample enhances its *ZT*.

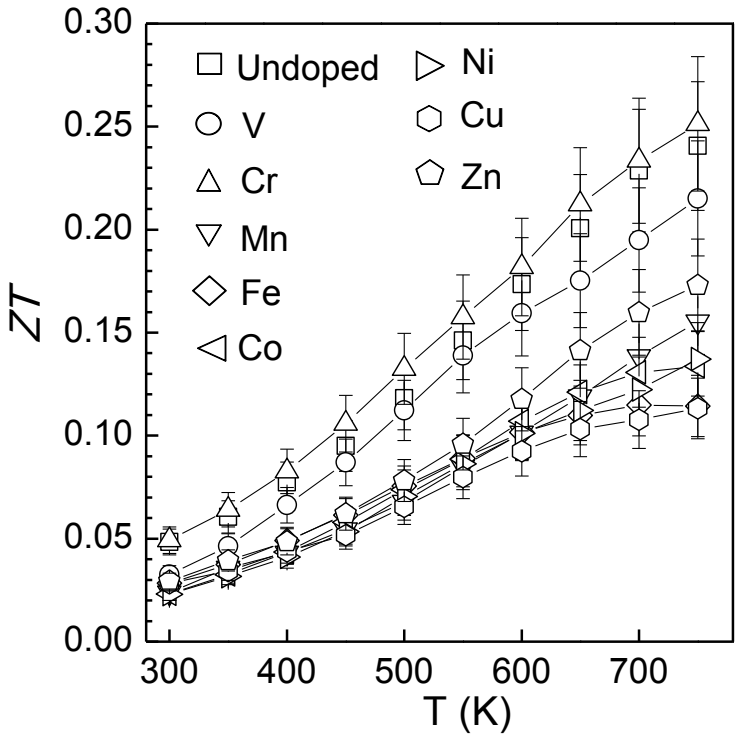

Figure 4-6. Dimensionless figure of merit (*ZT*) of TM doped samples. Considering the uncertainty in the measurements of electrical conductivity, Seebeck coefficient, thermal diffusivity and specific heat capacity, the error bars are a maximum of 13% for ZT.

4.4. Summary

In summary, we attempted to improve the thermoelectric properties of $(BiS)_{1.2}(TiS_2)_2$ misfit layer sulfides by TM substitution. It was hoped that TM substitution would reduce carrier concentration, which could lead to an increase in the Seebeck coefficient and *ZT* of the doped materials. All of the TM-doped samples had reduced carrier concentration compared with that of $(BiS)_{1.2}(TiS_2)_2$, but only V and Cr dopants led to a large increase in the Seebeck coefficient. The enhanced Seebeck coefficient of the V and Cr-doped samples was caused by the increase in the effective mass of carriers as a result of the change in electronic structure upon doping. The low energy level of the $3d_{t2g}$ half-filled orbitals of V and Cr possibly induced the formation of an additional or resonance state near the Fermi level in these samples. Although the lattice thermal conductivity could not be optimized, the decrease in electronic thermal conductivity obtained substantially reduced the total thermal conductivity of the V and Cr-doped samples, which enhanced *ZT*.

References

[1] Yanzhong Pei, Xiaoya Shi, Aaron LaLonde, Heng Wang, Lidong Chen, G. Jerry Snyder, Nature 473, 66 (2011).

[2] G. J. Snyder, E. S. Toberer, Nat. Mater. 7, 105 (2008).

[3] G.A. Slack, New Materials and Performance Limits for Thermoelectric Cooling, in: D.M. Rowe, CRC Handbook of Thermoelectric, CRC Press: Boca Raton, FL, USA (1995) pp. 407–440.

[4] Terry M. Tritt, Annu. Rev. Mater. Res. 41, 433 (2011).

[5] H. Imai, Y. Shimakawa,Y. Kubo, Phys. Rev. B. 64, 241104 (2001).

[6] C.H. Chen, W. Fabian, F.C. Brown, K.C. Woo, B. Davies, B. DeLong, Phys. Rev. B. 21, 615 (1980).

[7] J. A. Wilson, Phys. Stat. Sol (b) 86, 11 (1978).

[8] E. Guilmeau, Y. Breard, A. Maignan, Appl. Phys. Lett. 99, 052107 (2011).

[9] Chunlei Wan, Yifeng Wang, Ning Wang and Kunihito Koumoto, Materials 3, 2606 (2010).

[10] C.L. Wan, Y.F. Wang, N. Wang, Y.E. Putri, W. Norimatsu, M. Kusunoki, K. Koumoto, Layered Structure Metal Sulfides as Novel thermoelectric materials, in: D.M. Rowe, Modules, System and Application in Thermoelectric, CRC Press: Boca Raton, FL, USA, 2012, pp.4.1–4.11.

[11] Yulia Eka Putri, Chunlei Wan, Yifeng Wang, Wataru Norimatsu, Michiko Kusunoki and Kunihito Koumoto, Script. Mater. 66, 895 (2012).

[12] L.C. Otero-Diaz, R.L. Withers, A. Gomez-Herrero, T.R. Welberry and S. Schmid, J. Sol. State. Chem. 115, 274 (1995).

[13] W. Bensch and R. Schlögl, J. Solid State Chem. 107, 43 (1993).

[14] Toshihiro Kuzuya, Keiichi Itoh, Minoru Ichidate, Takahide Wakamatsu, Yasuhiro Fukunaka and Kenji Sumiyama, Electrochimica Acta 53, 213 (2007).

[15] M.C. Biesinger, C. Brown, J.R. Mycroft, R.D. Davidson and N.S. McIntyre, Surf. Interface Anal. 36, 1550 (2004).
[16] Tian Xi Wang and Wei Wei Chen, Chem. Eng. J. 144, 146 (2008).
[17] A.P. Grosvenor, B.A. Kobe, M.C. Biesinger and N.S. McIntyre, Surf. Interface Anal. 36, 1564 (2004).
[18] G.H. Yue, P.X. Yan, J.Z. Liu, X.Y. Fan and R.F. Zhuo, Appl. Phys. Lett. 87, 262505 (2005).
[19] Ning Chen, Wanqun Zhang, Weichao Yu, Yitai Qian, Mater. Lett. 55, 230 (2002).
[20] Wei Liu, Mater. Lett. 60, 551 (2006).
[21] J. Zhang, X.Y.Qin, H.X. Xin, D.Li, C.J.Song, J. Electron. Mater. 40, 980 (2011).
[22] M. Nistor, F. Gherendi, N. B. Mandache, C. Hebert, J. Perrière and W. Seiler, J. Appl. Phys. 106, 103710 (2009).
[23] H. Kozuka, K. Yamagiwa, K. Ohbayashi, K. Koumoto, J. Mater. Chem. 22, 11003 (2012).
[24] M.D. Nielsen, E.M. Levin, C.M. Jaworski, K. Schmidt-Rohr and J.P. Heremans, Phys. Rev. B 85, 045210 (2012).
[25] Christopher M. Jaworski, Bartlomiej Wiendlocha, Vladimir Jovovic and Joseph P. Heremans, Energy Environ. Sci. 4, 4155 (2011).
[26] J. Zhang, X.Y. Qin, D. Li, H.X. Xin, L. Pan, K.X. Zhang, J. Alloy Compd.479, 816 (2009).
[27] Chunlei Wan, Yifeng Wang, Wataru Norimatsu, Michiko Kusunoki and Kunihito Koumoto, Appl. Phys. Lett.100, 101913 (2012).

Chapter V

Thermoelectric Properties Enhancement of $(BiS)_{1.2}(TiS_2)_2$ Misfit Layer Sulfide by Chromium Doping

5.1. Preface

We have successfully found an appropriate acceptor dopant for $(BiS)_{1.2}(TiS_2)_2$ from our previous work. The chromium doping has successfully reduced the carrier concentration with reduction of electrical conductivity; in the mean time also enhanced the Seebeck coefficient and the effective mass. Although, the formation of ordered structure was taking place in the chromium doped samples resulted an increase in lattice thermal conductivity but low electronic thermal conductivity due to the decrease in the electrical conductivity has contributed to the low thermal conductivity. As a result, the final *ZT* value was improved. We assumed that the increase of Seebeck coefficient can be attributed to the formation of additional or resonant states near the Fermi level [1,2]. In this study, we fabricate a series chromium doped sample with several doping level to investigate the optimal doping level for $(BiS)_{1.2}(TiS_2)_{2.}$ In addition, for further investigation, we carried out the DFT calculation to confirm the formation of additional or resonant states in the chromium doped sample.

5.2. Experimental procedure

The powder samples were synthesized by using solid state reaction method. The sample preparation and procedure have been reported in our previous work (chapter I). All pellets obtained from spark plasma sintering (SPS) have relatively high density of over 96%. We measured thermoelectric properties along the direction perpendicular to the pressure applied during the sintering process. XRD measurements helped analyze the phase composition (RINT-2100, Rigaku). The ionic state of chromium was analyzed via XPS (JEOL, Al kα source). In order to clarify the effective mass change after Cr doping, the density of states (DOS) of samples calculated using the density functional theory as implemented in the Quantum-ESPRESSO package.

5.3. Results and discussion

5.3.1. Morphology observation and structural analysis

The morphology of the pellet samples are shown in the Fig. 5-1. The plate like particles are well-align in the direction perpendicular to the pressure applied during sintering. SEM image shows that the samples are dense and the relative density is over 97%.

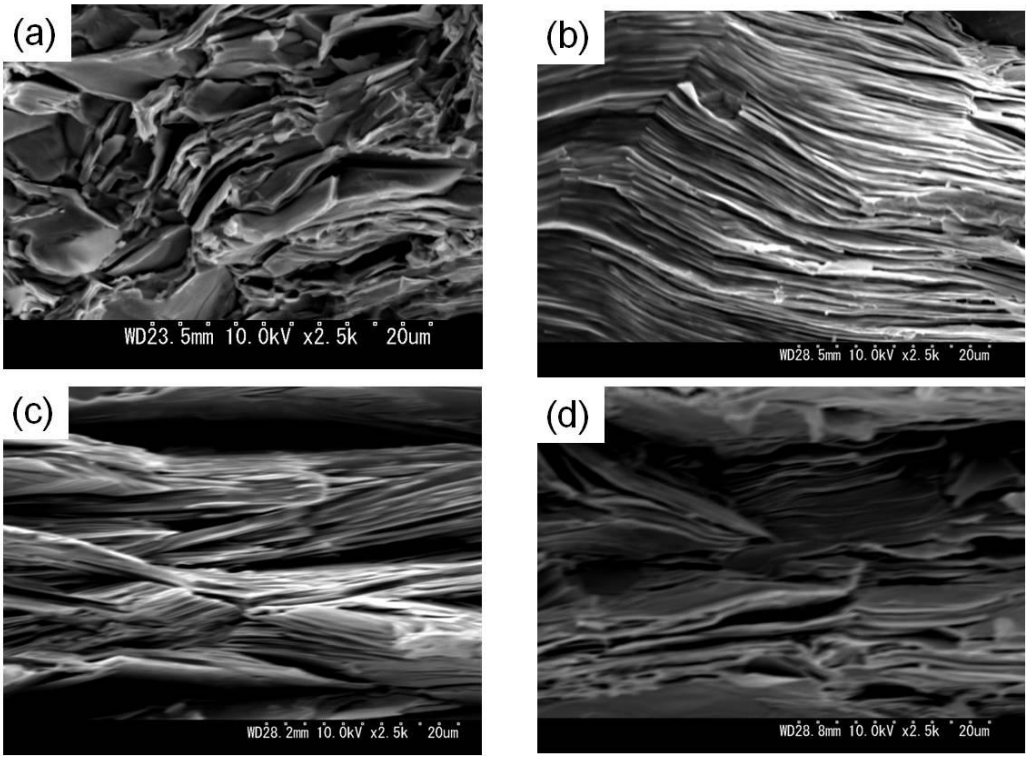

Fig. 5-1. SEM images of $(BiS)_{1.2}(Ti_{1-x}Cr_xS_2)_2$ pellet samples. (a) Undoped, (b) x = 0.025, (c) x = 0.05 and (d) x = 0.1.

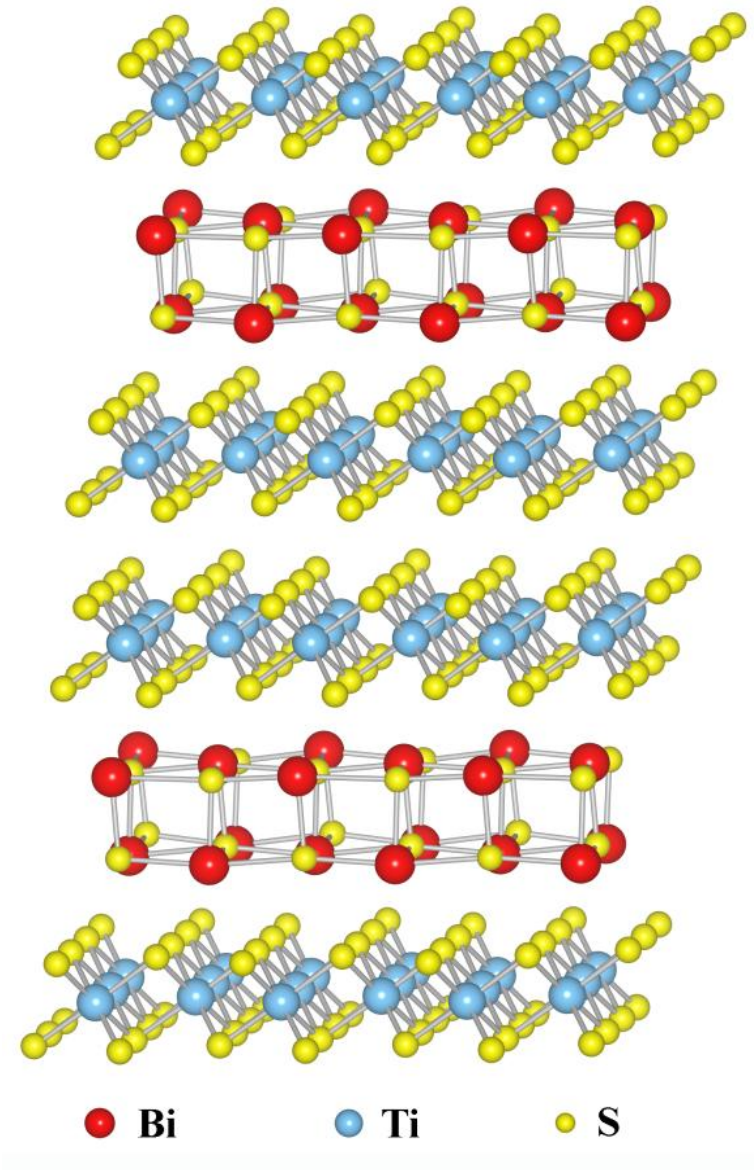

Fig. 5-2. The natural superlattice structure of $(BiS)_{1.2}(TiS_2)_2$ misfit layer sulfide.

Fig. 5-2 shows that pure $(BiS)_{1.2}(TiS_2)_2$ has a natural superlattice structure, in which double TiS_2 layers and one BiS layer stack alternatively in the c-axis direction. Cr^{3+} (0.63 Å) was intended as a substitute at the Ti^{4+} (0.68 Å) site, rather than the Bi^{3+} (0.96 Å) site. XRD patterns of the pellets were observed in the direction perpendicular to the applied pressure during the sintering process and are shown in Fig.5-3. Several strong peaks demonstrate that all the samples have a high degree of (00*l*) orientation. The peaks of chromium-doped misfit layer sulfides (x = 0.025, 0.05, 0.1) correspond to those of the undoped (x = 0) sample, proving that the chromium-doped misfit layer sulfide $(BiS)_{1.2}(Ti_{1-x}Cr_xS_2)_2$ has a crystal structure related to that of $(BiS)_{1.2}(TiS_2)_2$[3]. No substantial changes were observed in the XRD pattern of the chromium-substituted compound, with only a slight shift to higher angles at around 27 degrees (00$\underline{10}$), indicating that the layer spacing *c* in the doped misfit layer sulfide shortened linearly from 16.9665 Å to 16.6849 Å, as the doping level *x* increased from 0 to 0.1.

5.3.2. Ionic state analysis

Furthermore, we have performed XPS measurements to identify the ionic state of the chromium dopant. Fig. 5-4 shows the XRF spectra for all doped samples. As a reference standard for chromium (III), we also measured chromium (III) sulfide (Cr_2S_3); its XRF spectrum is shown in the lower part of the figure. The Cr $2p_{3/2}$ spectrum is shown for reference, at a binding energy (BE) of 573 eV. The peak positions of samples with Cr concentration of x = 0.05 and 0.1 are quite similar to that of Cr (III) in Cr_2S_3, which implies that the Cr is nearly trivalent [4,5]. This proves that the Cr^{3+} has been successfully substituted into Ti^{4+} octahedral sites in the TiS_2 layers.

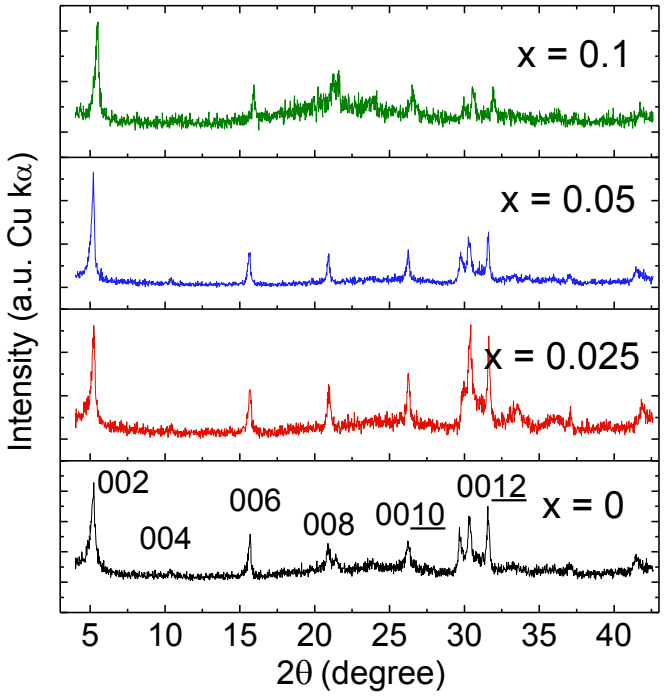

Fig. 5-3. XRD pattern for $(BiS)_{1.2}(Ti_{1-x}Cr_xS_2)_2$ (x = 0, 0.025, 0.05, and 0.1).

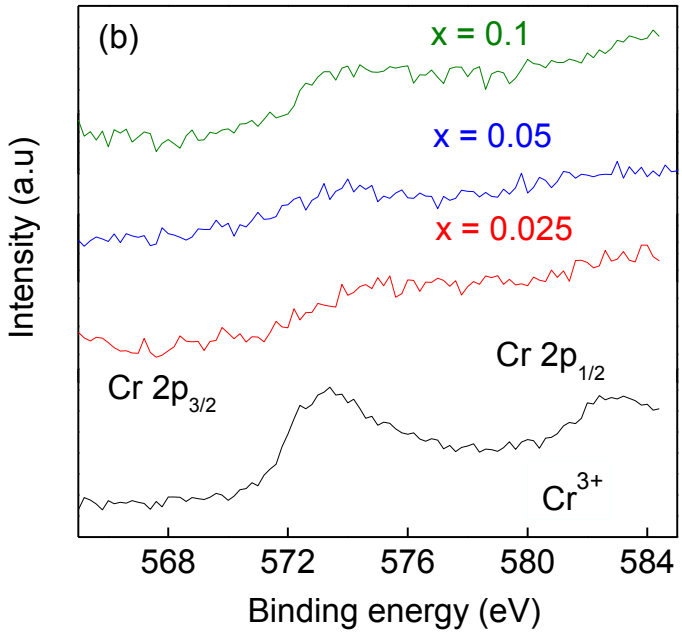

Fig. 5-4. XPS Spectra for $(BiS)_{1.2}(Ti_{1-x}Cr_xS_2)_2$ (x = 0, 0.025, 0.05, and 0.1).

5.3.3. Thermoelectric properties

5.3.3.1. Electrical conductivity

Figure 5-5(a) shows that chromium doping into titanium sites in the TiS_2 layers significantly reduces the electrical conductivity in the whole temperature range studied. The decrease in electrical conductivity is in agreement with the increase in chromium doping levels. Furthermore, all compounds depicting this kind of change in electrical conductivity are metallic conductors [6-8]. The electrical conductivity of a material is determined by its carrier concentration and mobility. Therefore, we have carried out Hall measurements to examine carrier concentrations, so as to clarify the decrease in electrical conductivity. The carrier concentration of all samples decreased, as shown in Fig.5-5(b).

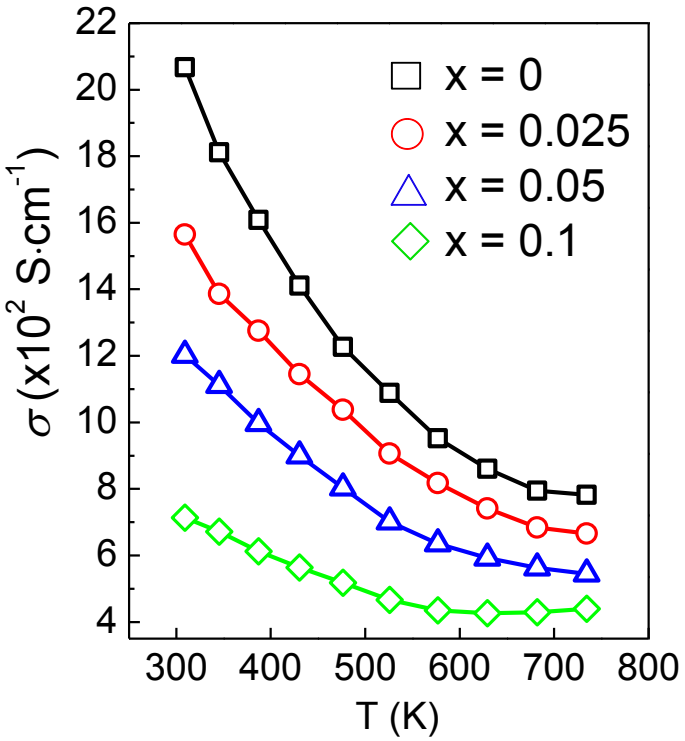

Fig. 5-5. Electrical conductivity of $(BiS)_{1.2}(Ti_{1-x}Cr_xS_2)_2$ (x = 0, 0.025, 0.05, and 0.1).

The carrier concentration of all samples decreased, as shown in Fig.5-6. These results confirm that chromium doping reduces carrier concentration, which is consistent with the change in electrical conductivity of the samples.

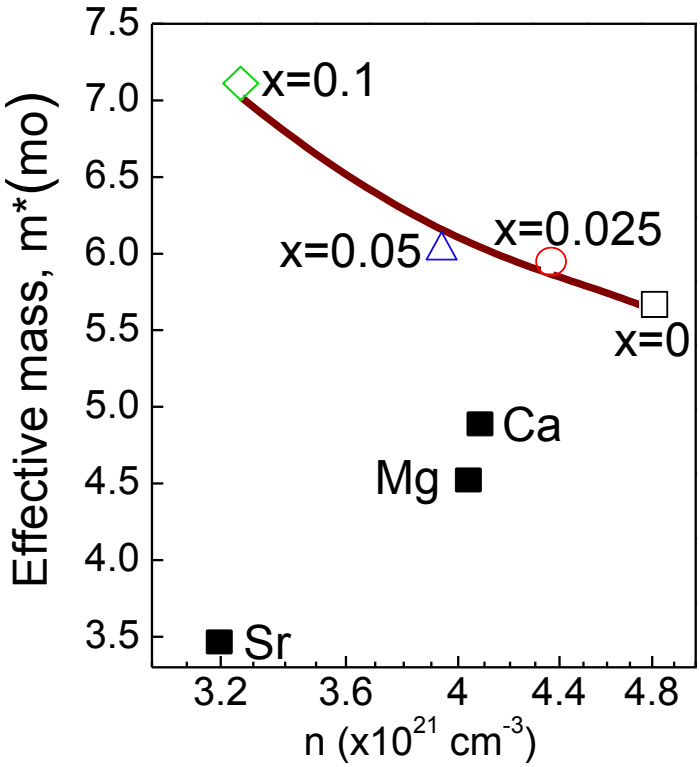

Fig. 5-6. The change in effective mass as a function of carrier concentration

Figure 5-7 is Hall mobility of carriers as a function of temperature of each chromium doped sample. The mobility for x = 0 has a temperature dependence proportional to $T^{-1.5}$, indicating the dominance of electron scattering by acoustic phonons [9-11]. However, increasing the chromium doping amount leads to a decrease in the dependence of mobility on temperature. This implies that, in addition to acoustic phonon scattering, ionized impurity scattering or alloy scattering also takes place [12,13].

5.3.3.2. Seebeck coefficient

The samples show negative Seebeck coefficients, meaning that electrons are the main carriers, as shown in Fig. 5-8. The samples with chromium doping show higher Seebeck coefficients. The general expression for the Seebeck coefficient is as follows [14]:

$$S = \frac{8\pi^2 k_B^2}{3eh^2} m^* T \left\{ \frac{\pi}{3n} \right\}^{2/3}, \quad (5\text{-}1)$$

where n is the carrier concentration, m^* is the effective mass of the carrier, k_B is the Boltzmann constant (1.381×10^{-23} JK^{-1}), h is the Plank constant (6.626×10^{-34} m^2kgs^{-1}), e is the electron charge (1.602×10^{-19} C), and T is the temperature (K).

The increase in Seebeck coefficient with chromium doping is mainly due to the decrease in carrier concentrations, n. Moreover, we should also point out that the effective mass shows a systematic increase with increasing doping levels, which further contributes to the increase in the Seebeck coefficient, as shown in Fig. 5-5(b). This is different from our previous study, in which the alkaline earth metal doping ($(BiS)_{1.2}(Ti_{0.95}Mg_{0.05}S_2)_2$, $(Bi_{0.9}Ca_{0.1}S)_{1.2}(TiS_2)_2$, and $(Bi_{0.9}Sr_{0.1}S)_{1.2}(TiS_2)_2$) and transition metal doping ($(BiS)_{1.2}(Ti_{0.95}TM_{0.05}S_2)_2$ (TM: Mn,Co,Fe,Ni,Zn)) decreased the effective mass.

It is believed that pure $(BiS)_{1.2}(TiS_2)_2$ has a non-parabolic band structure, such that the decrease in carrier concentration can reduce the effective mass [15,16]. In the case of chromium doping, however, the effective mass increases as the carrier concentration decreases, which may be due to the formation of additional states near the Fermi level; further investigation is needed to prove this assumption.

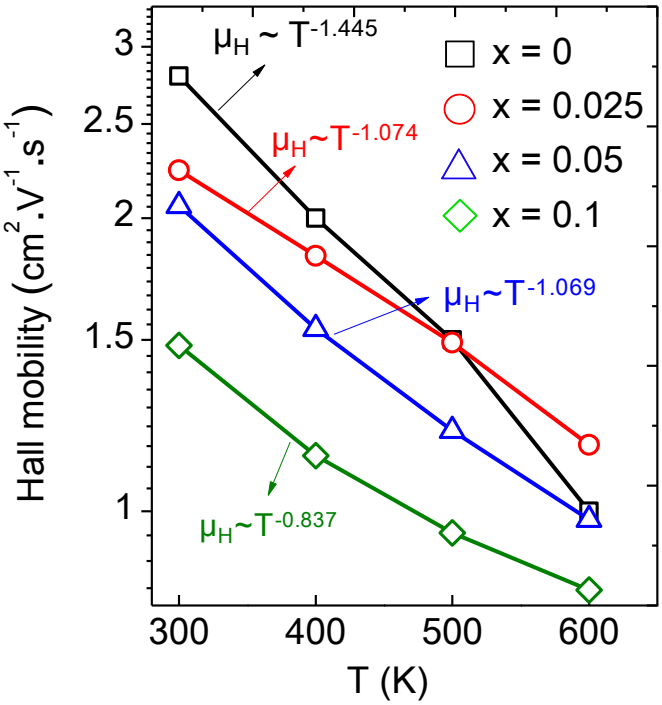

Fig. 5-7 Hall mobility of $(BiS)_{1.2}(Ti_{1-x}Cr_xS_2)_2$ (x = 0, 0.025, 0.05, and 0.1).

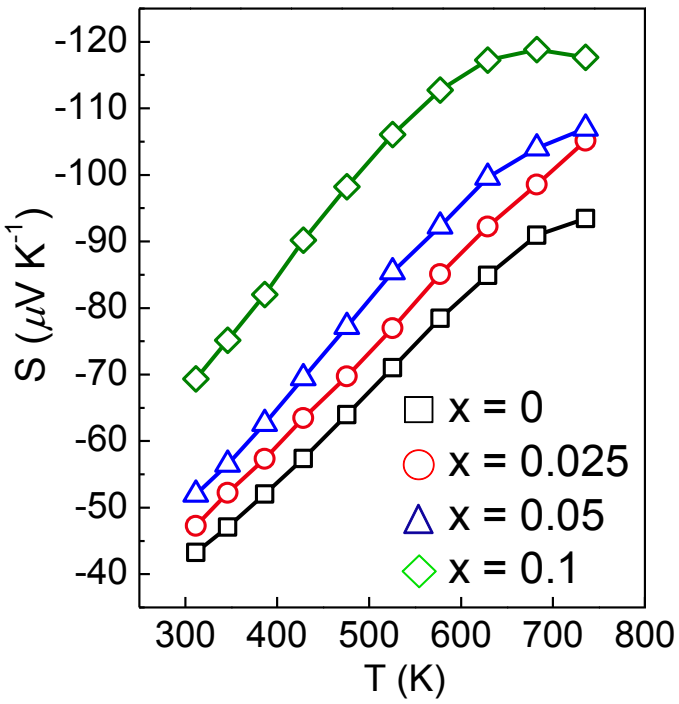

Fig.5-8. Seebeck coefficient of $(BiS)_{1.2}(Ti_{1-x}Cr_xS_2)_2$ (x = 0, 0.025, 0.05, and 0.1).

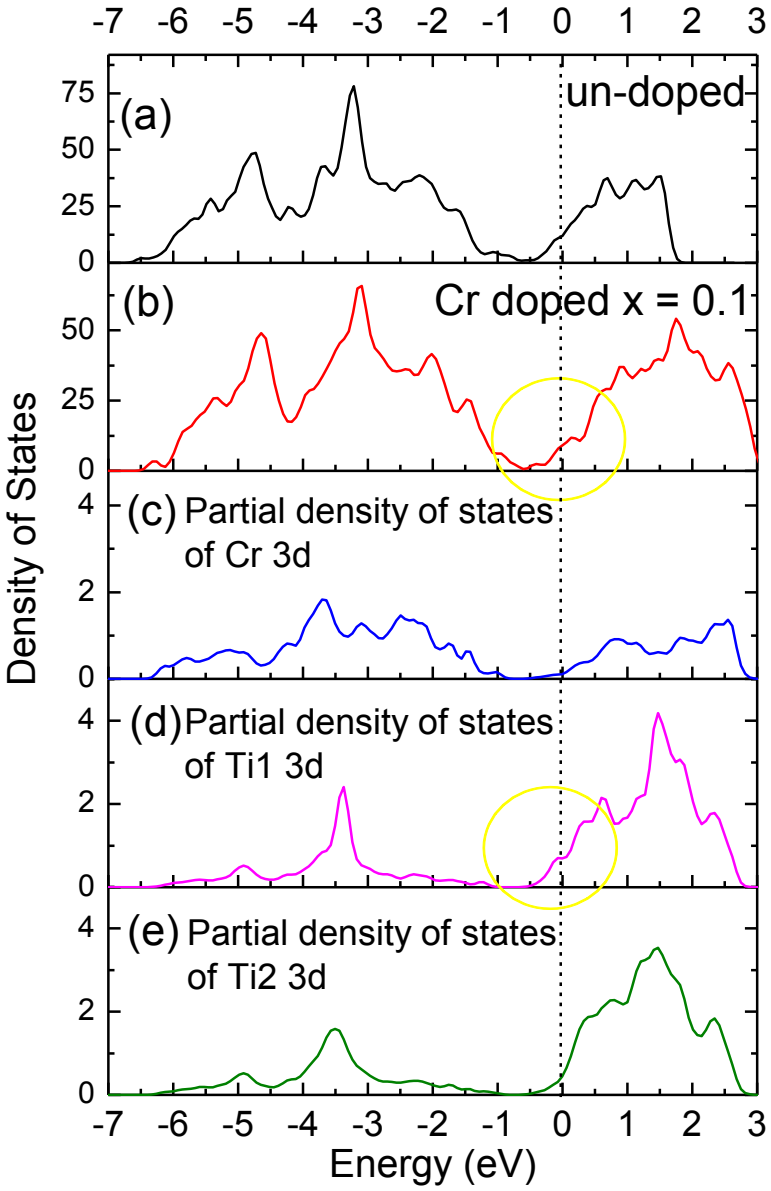

Fig. 5-9. The total density of states of (a) un-doped and (b) $(BiS)_{1.2}(Ti_{0.9}Cr_{0.1}S_2)_2$. Partial density of states of (c) Cr *3d*, (d) Ti_1 *3d* and (e) Ti_2 *3d*. Ti_1 means Ti atom near the Cr dopant and Ti_2 means Ti atom far from the Cr dopant.

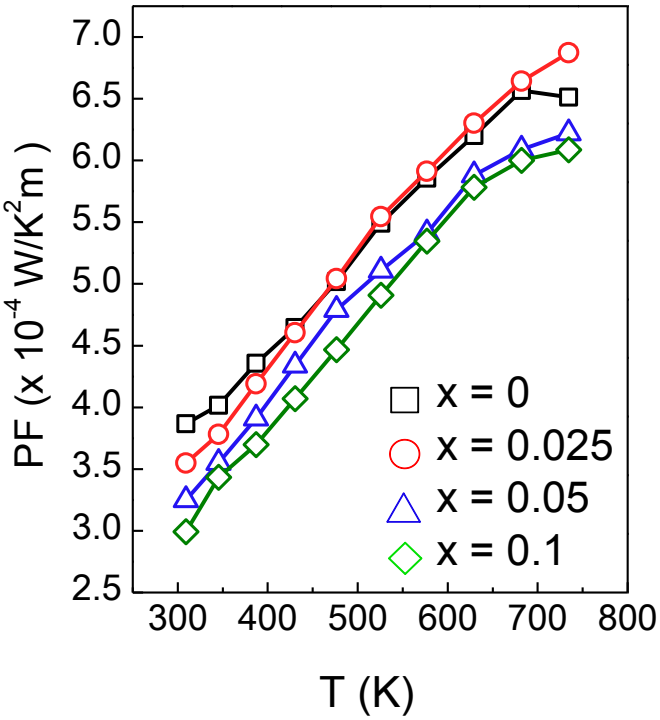

Fig.5-10. Power factor of $(BiS)_{1.2}(Ti_{1-x}Cr_xS_2)_2$ (x = 0, 0.025, 0.05, and 0.1).

5.3.3.3. Density of states (DOS) calculation

In order to clarify the effective mass change by Cr doping, the density of states (DOS) of un-doped and 10% Cr-doped $(BiS)_{1.2}(TiS_2)_2$ misfit layer sulfide were both calculated by using the density functional theory as implemented in the Quantum-ESPRESSO package [17,18]. The results are shown in Fig.5-9.The Fermi levels, indicated by the dotted line, were calculated by using the Fermi integral from the carrier concentrations shown in Fig 5-6. From Fig.5-9 (a) and (b), it can be seen that the DOS near the Fermi level is enlarged by Cr doping. This enlargement results in a larger carrier effective mass, which agrees with the trends shown in Fig.5-6. Moreover, the DOS near the Fermi level is mainly contributed by the *3d* orbitals of Ti atoms near the Cr dopant, as shown in Fig.5-9 (c), (d) and (e).

Figure 5-10 depicts the power factor calculated from their measured electrical conductivity and Seebeck coefficient. It shows that chromium doping cannot optimize the power factor due to the large decrease in electrical conductivity despite the higher Seebeck coefficient.

5.3.3.4. Thermal conductivity

The total thermal conductivity of chromium-doped samples with different chromium doping level decreases in the whole temperature range. This significant decrease is mainly due to the decrease in electronic thermal conductivity, as shown in Fig. 5-11(a). In the case of $(BiS)_{1.2}(TiS_2)_2$, κ_e contributes more to κ than κ_l [19,20]. This is also the case for x = 0.025 samples. However, for the sample with x = 0.05 and 0.1, the point where κ_l contributes more to κ compared to κ_e, differs from that of the previous samples. Furthermore, chromium doping leads to different effects on the lattice thermal conductivity of the samples, as shown in Fig. 5-11(b). The samples with x = 0.05 and 0.1 show an increase in lattice thermal conductivity. This enhancement is probably due to a new structural ordering as a result of eliminating of planar stacking faults [21]. The resulting ordered structure should have weaker phonon scattering than the disordered $(BiS)_{1.2}(TiS_2)_2$ with planar stacking faults, and thus should have enhanced lattice thermal conductivity [22-24]. On the other hand, κ_l for the sample with x = 0.025 decreases due to the absence of structural ordering; as a result, this sample could have reduced total thermal conductivity compared to the samples with x = 0.05.

The sound velocity measurement was carried out to examine the effect of structural ordering formation on the lattice thermal conductivity. Table 5-1 show that V_L have different values for each doping level, attributed to the different values of density. The V_{T1} and V_{T2} of the samples with x = 0.05 and 0.1 increased, while for the x = 0.025 sample

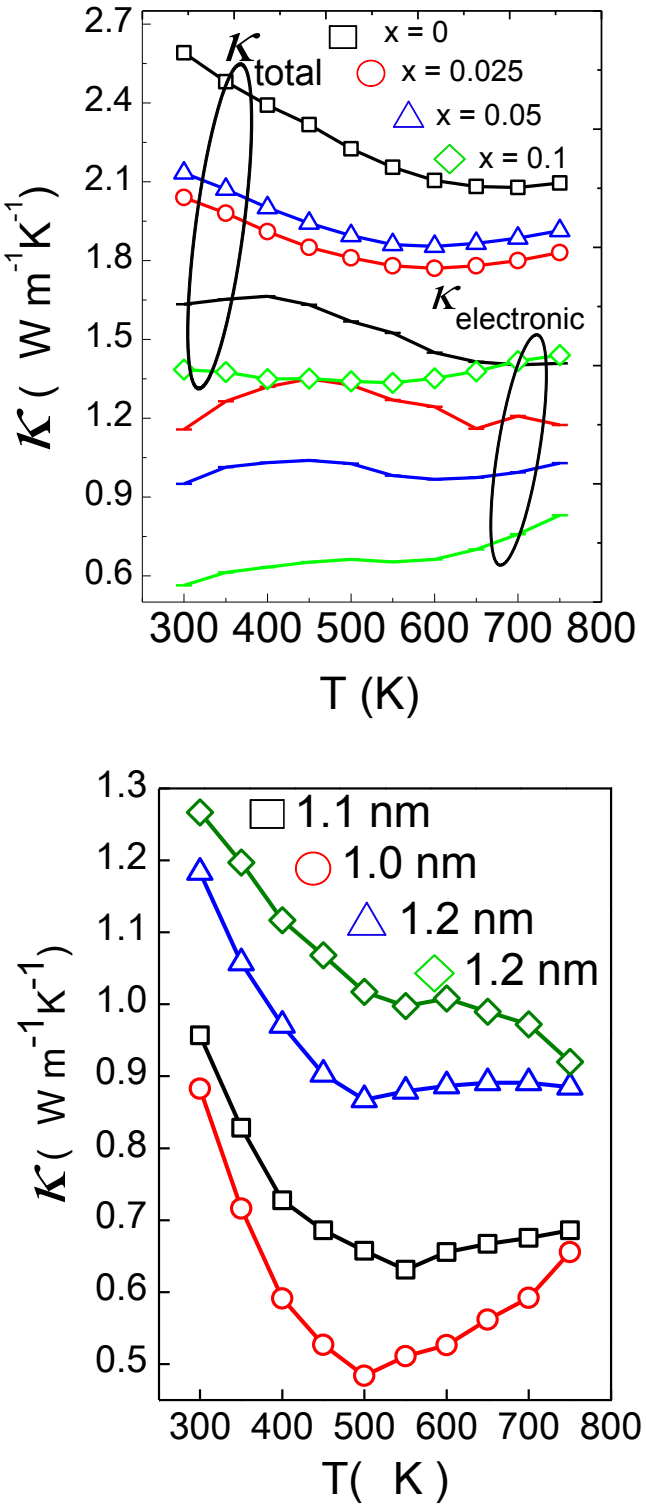

Fig. 5-11. Thermal conductivity (a) The total thermal conductivity and (b) the lattice thermal conductivity of $(BiS)_{1.2}(Ti_{1-x}Cr_xS_2)_2$ (x = 0, 0.025, 0.05, and 0.1).

they decreased. The increase in V_{T2} in the samples with x = 0.05 and 0.01 was predicted due to the strengthening of covalent bonding between chromium atoms and the sulfur atoms within the TiS_2 layers. The increase in V_{T2} is thought to be due to reinforced intralayer bonding, as a result the lattice thermal conductivity is enhanced. On the contrary, the V_{T1} and V_{T2} of the x = 0.025 samples decreased due to the softening of the interlayer bonding and the weakening of intralayer bonding, and, as a result, the lattice thermal conductivity decreased.

Table 5-1. Density, V_L, V_{T1}, V_{T2} of $(BiS)_{1.2}(Ti_{1-x}Cr_xS_2)_2$ (x = 0, 0.025, 0.05, and 0.1).

Sample	ρ (gcm^{-3})	V_L (ms^{-1})	V_{T1} (ms^{-1})	V_{T2} (ms^{-1})
x = 0	4.4	3596	1396	1660
x = 0.025	4.2	3860	1375	1580
x = 0.05	4.4	3515	1502	1693
x = 0.1	4.3	3580	1698	1931

5.3.3.5. Dimensionless figure of merit (*ZT*)

Figure 5-12 shows the *ZT* value calculated from the measured electrical conductivity, Seebeck coefficient, and thermal conductivity. All chromium-doped samples exhibit an increase in *ZT* of 0.24–0.3 at a temperature of 750 K. Although the chromium substitution did not result in higher power factor, its low total thermal conductivity contributed to an increase in *ZT*.

5.4. Summary

In this work we have successfully improved the thermoelectric properties of $(BiS)_{1.2}(TiS_2)_2$ misfit layer sulfides through the optimization of carrier concentration by chromium doping. The chromium ions substituted for the titanium sites reduced the carrier concentration and increased the Seebeck coefficient. Unlike other acceptor dopants, chromium increased the effective mass, which further enhanced the Seebeck coefficient. It is assumed that additional resonant states may be formed near the Fermi level which can account for the increase in effective mass and further investigation is required in the near future. The electronic thermal conductivity was significantly reduced due to the decrease in electrical conductivity. Consequently, the overall *ZT* value measurably improved, even though the power factor decreased slightly.

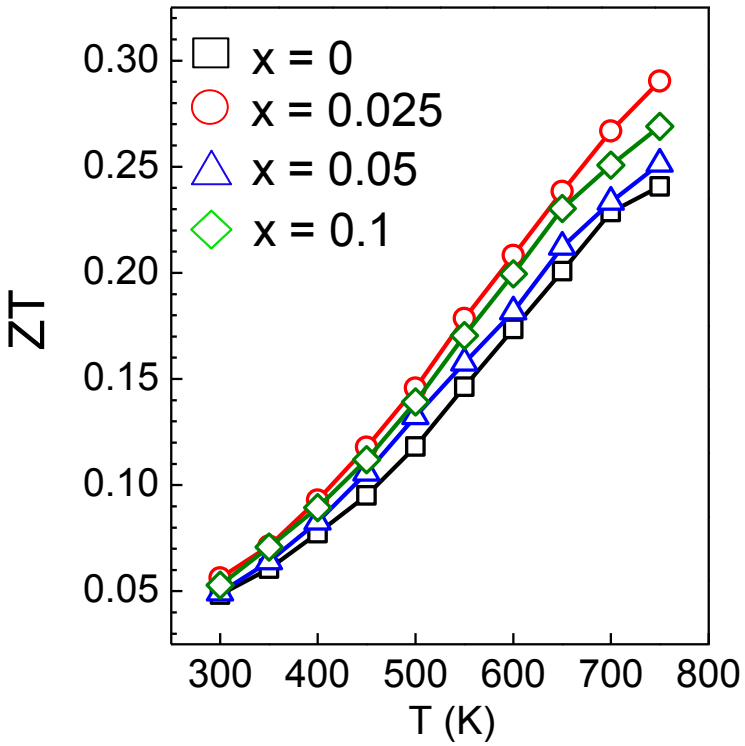

Fig. 5-12. The dimensionless figure of merit *ZT* for $(BiS)_{1.2}(Ti_{1-x}Cr_xS_2)_2$ (x = 0, 0.05, and 0.1).

References

[1] M.D. Nielsen, E.M. Levin, C.M. Jaworski, K. Schmidt-Rohr and J.P. Heremans, Phys. Rev. B 85 (2012) 045210-1-045210-7.

[2] Christopher M. Jaworski, Bartlomiej Wiendlocha, Vladimir Jovovic and Joseph P. Heremans, Energy Environ. Sci. 4 (2011) 4155-4162.

[3] Chunlei Wan, Yifeng Wang, Ning Wang and Kunihito Koumoto, Materials 3 (2010) 2606–2617.

[4] E. Unveren, E. Kemnitz, S. Hutton, A. Lippitz and W. E. S. Unger, Surf. Interface Anal. 36 (2004) 92-95.

[5] M.C. Biesinger, C. Brown, J.R. Mycroft, R.D. Davidson and N.S. McIntyre, Surf. Interface Anal. 36 (2004) 1550-1563.

[6] J. Zhang, X.Y.Qin, H.X. Xin, D.Li, C.J.Song, J. Electron. Mater. 40 (2011) 980-986.

[7] R. Dingle, H. L. Stormer, A. C. Gossard and W. Wiegmann, Appl. Phys. Lett. 33 (1978) 665-667.

[8] John Y. W. Seto, J. Appl. Phys. 46 (1975) 5247-5254.

[9] S.M. Sze, Semi Conductor Devices, 2nd ed., Wiley, USA, 2001:

[10] G.A. Wiegers, J. Alloys Compd. 219 (1995) 152–156.

[11] P.P. Debye and E.M. Conwell, Phys. Rev. 93 (1994) 693-706.

[12] L. Tichy, M. Frumar, M. Kincl, J. Klikorka, A. Trfska, Phys. Stat. Sol (a) 64 (1981) 461-466.

[13] E. Flage Larsen and O. Prytz, Appl. Phys. Lett. 99 (2011) 202108.

[14] G. J. Snyder, E. S. Toberer, Nat. Mater. 7 (2008) 105-114.

[15] J.O. Sofo and G.D. Mahan, Phys. Rev. B 58 (1998) 15620–15623.

[16] J. Wu, W. Walukiewicz, W. Shan, K. M. Yu, J. W. Ager III, E. E. Haller, Hai Lu and William J. Schaff, Phys. Rev.B 66 (2002) 201403-1-201403-4.

[17] P. Giannozzi, S. Baroni, N. Bonini, M. Calandra, R. Car, C. Cavazzoni, D. Ceresoli, G.L. Chiarotti, M. Cococcioni, I. Dabo, A.D. Corso, Sd.

Gironcoli, S. Fabris, G. Fratesi, R. Gebauer, U. Gerstmann, C. Gougoussis, A. Kokalj, M. Lazzeri, L. Martin-Samos, N. Marzari, F. Mauri, R. Mazzarello, S. Paolini, A. Pasquarello, L. Paulatto, C. Sbraccia, S. Scandolo, G. clauzero, A.P. Seitsonen, A. Smogunov, P. Umari, and R.M. Wentzcovitch, J. Phys.: Condens.Matter. 21, 395502 (2009).

[18] R.Z. Zhang, C.L. Wang, J.C. Li, W.B. Su, J.L. Zhang, M.L.Zhao, J.A. Liu, Y.F. Zhang, and L.M. Mei, Solid State Sci.12 (2010) 1168-1172.

[19] J. Zhang, X.Y. Qin, D. Li, H.X. Xin, L. Pan, K.X. Zhang, J. Alloy Compd. 479 (2009) 816-820.

[20] A. J. Minnich, M. S. Dresselhaus, Z. F. Ren and G. Chen, Energy & Environ. Sci. 2 (2009) 466-479.

[21] C.L. Wan, Y.F. Wang, N. Wang, Y.E. Putri, W. Norimatsu, M. Kusunoki, K. Koumoto, Layered Structure Metal Sulfides as Novel thermoelectric materials, in: D.M. Rowe, Modules, System and Application in Thermoelectric, CRC Press: Boca Raton, FL, USA, (2012) 4.1–4.11.

[22] Chunlei Wan, Yifeng Wang, Wataru Norimatsu, Michiko Kusunoki and Kunihito Koumoto, Appl. Phys. Lett. 100 (2012) 101913-1-101913-4.

[23] David G. Cahill and S. K. Watson and R. O. Pohl, Phys. Rev B 46 (1992) 6131-6140.

[24] Yulia Eka Putri, Chunlei Wan, Yifeng Wang, Wataru Norimatsu, Michiko Kusunoki and Kunihito Koumoto, Script. Mater. 66 (2012) 895-898.

Chapter VI

The Future of Misfit Layer Sulfide as Thermoelectric Materials

The study on $(Bi_{1-y}B_yS)_n$ $(Ti_{1-x}A_xS_2)_2$ misfit layer sulfide as a novel thermoelectric material reveals that the thermoelectric performance of this compound can be improved by dope of low valency dopants, as so called the modulation or selective doping. We have tried to dope several dopants from alkaline earth elements and transition metal elements into the different layer; host layer TiS_2 or phonon barrier layer BiS. In this work we have successfully improved the thermoelectric properties of $(BiS)_{1.2}(TiS_2)_2$ misfit layer sulfide through the optimization of carrier concentration by chromium doping. The chromium ions substituted for the titanium sites reduced the carrier concentration and increased the Seebeck coefficient. Unlike other acceptor dopants, chromium increased the effective mass, which further enhanced the Seebeck coefficient. It is assumed that additional resonant states may be formed near the Fermi level which can account for the increase in effective mass and further investigation is required in the near future. The electronic thermal conductivity was significantly reduced due to the decrease in electrical conductivity. Consequently, the overall *ZT* value measurably improved

Good thermoelectric materials have high electrical conductivity and Seebeck coefficients and low thermal conductivities, but these properties are not independent. In particular, the electrical conductivity and Seebeck coefficient are inversely related, so it is not generally possible to increase the thermoelectric power factor above a particular optimal value for a bulk material. We realized that the enhancement of thermoelectric properties in our samples due to the increase in electrical properties; the decrease in electrical conductivity led to significant increase in Seebeck coefficient. However, another parameter, thermal conductivity, could not be maintained in the ultra low value. Even though, the electronic thermal conductivity can be lowered due to the decrease in electrical conductivity but an increase in

lattice thermal conductivity caused high total thermal conductivity. We found that the enhancement of lattice thermal conductivity due to a new structural ordering as a result of eliminating of planar stacking faults and the formation of ordered structure. These reasons should have weaker phonon scattering than the disordered $(BiS)_{1.2}(TiS_2)_2$ with planar stacking faults, and thus should have enhanced lattice thermal conductivity. Therefore, further investigation are required on how to retain the ultra low lattice thermal conductivity in the $(BiS)_{1.2}(TiS_2)_2$ misfit layer sulfide to achieve a high *ZT* value.

LIST OF PUBLICATION

RESEARCH PAPERS

1. **Yulia Eka Putri**, Chunlei Wan, Yifeng Wang, Wataru Norimatsu, Michiko Kusunoki and Kunihito Koumoto, Effects of Alkaline Earth Doping on the Thermoelectric Properties of Misfit Layer Sulfides, *Script. Mater.* 66 (2012) 895-898.
2. **Yulia Eka Putri,** Chunlei Wan, Ruizhi Zhang, Takao Mori and Kunihito Koumoto, Thermoelectric Performance Enhancement of $(BiS)_{1.2}(TiS_2)_2$ Misfit Layer Sulfide by Chromium Doping, J. Adv. Ceramics. 2 (2013) 42-48.
3. **Yulia Eka Putri**, Chunlei Wan, Feng Dang, Takao Mori, Yuto Ozawa, Wataru Norimatsu, Michiko Kusunoki and Kunihito Koumoto, Effects of Transition Metal Substitution on the Thermoelectric Properties of Metallic $(BiS)_{1.2}(TiS_2)_2$ Misfit Layer Sulfides, *J. Electron. Mater.* In press DOI: 10.1007/s11664-013-2894-3.

BOOK

1. C.L. Wan, Y.F. Wang, N. Wang, **Y.E. Putri**, W. Norimatsu, M. Kusunoki, K. Koumoto, Layered Structure Metal Sulfides as Novel thermoelectric materials, in: D.M. Rowe, Modules, System and Application in Thermoelectric, CRC Press: Boca Raton, FL, USA, 2012:4.1–4.11.
2. C.L. Wan, Y.F. Wang, **Y.E. Putri** and K. Koumoto, Natural Superlattice Material: TiS_2-based Misfit Layer Compounds in: Thermoelectric Nanomaterials: Material design and Application, Springer Series in Materials Science, Springer-Verlag Berlin Heidelberg, 2013:8.157–.173.

LIST OF AWARDS

1. The ITS Outstanding Scientific Poster, The 30th International Conference on Thermoelectrics**,** July 17-21, 2011, Michigan, USA.
2. Excellent Poster Award at Electronic Ceramic Session, The 24th Annual Meeting of The Ceramic Society of Japan, September 7-9, 2011, Hokkaido, Japan.
3. Encouragement of Research 2011 Award, Material Backcasting Technology Symposium, October 31, 2011, Nagoya, Japan.
4. Young Researcher Award, Japan-France Joint Seminar on new concept for nano-structured thermoelectric oxides, November 9-10, 2011, Nagoya, Japan.
5. Poster Award, NTTHU (Nagoya Univ., Tsinghua Univ., Toyota Motor Corp., Hokkaido Univ., Univ. Electron. Sci. Tech. China) Joint Symposium, December 21-23, 2011, Chengdu, PR China.